

The resolution sensitivity of Northern Hemisphere blocking in four 25-km atmospheric global circulation models

Article

Accepted Version

Schiemann, R. ORCID: <https://orcid.org/0000-0003-3095-9856>, Demory, M.-E., Shaffrey, L. C. ORCID: <https://orcid.org/0000-0003-2696-752X>, Strachan, J., Vidale, P. L. ORCID: <https://orcid.org/0000-0002-1800-8460>, Mizielinski, M. S., Roberts, M. J., Matsueda, M., Wehner, M. F. and Jung, T. (2017) The resolution sensitivity of Northern Hemisphere blocking in four 25-km atmospheric global circulation models. *Journal of Climate*, 30 (1). pp. 337-358. ISSN 1520-0442 doi: <https://doi.org/10.1175/JCLI-D-16-0100.1> Available at <https://centaur.reading.ac.uk/67227/>

It is advisable to refer to the publisher's version if you intend to cite from the work. See [Guidance on citing](#).

Published version at: <http://dx.doi.org/10.1175/JCLI-D-16-0100.1>

To link to this article DOI: <http://dx.doi.org/10.1175/JCLI-D-16-0100.1>

Publisher: American Meteorological Society

All outputs in CentAUR are protected by Intellectual Property Rights law, including copyright law. Copyright and IPR is retained by the creators or other copyright holders. Terms and conditions for use of this material are defined in the [End User Agreement](#).

www.reading.ac.uk/centaur

CentAUR

Central Archive at the University of Reading

Reading's research outputs online

1 **The resolution sensitivity of Northern Hemisphere blocking in four 25-km**
2 **atmospheric global circulation models**

3 Reinhard Schiemann*, Marie-Estelle Demory, Len C. Shaffrey, Jane Strachan[†], Pier Luigi Vidale

4 *National Centre for Atmospheric Science, Department of Meteorology, University of Reading,*
5 *United Kingdom*

6 Matthew S. Mizieliński and Malcolm J. Roberts

7 *Met Office Hadley Centre, Exeter, United Kingdom*

8 Mio Matsueda

9 *Center for Computational Sciences, University of Tsukuba, Japan, and Department of Physics,*
10 *University of Oxford, United Kingdom*

11 Michael F. Wehner

12 *Lawrence Berkeley National Laboratory, Berkeley, California, USA*

13 Thomas Jung

14 *ECMWF, Reading, United Kingdom, and AWI, Bremerhaven, Germany*

15 *Corresponding author address: R. Schiemann, NCAS-Climate, Department of Meteorology, Uni-
16 versity of Reading, Earley Gate, PO Box 243, Reading RG6 6BB, United Kingdom.

17 E-mail: r.k.schiemann@reading.ac.uk

¹⁸ †Current affiliation: Met Office Hadley Centre, Exeter, United Kingdom.

ABSTRACT

19 The aim of this study is to investigate if the representation of Northern Hemi-
20 sphere blocking is sensitive to resolution in current-generation atmospheric
21 global circulation models (AGCMs). An evaluation is conducted of how well
22 atmospheric blocking is represented in four AGCMs whose horizontal reso-
23 lution is increased from a grid spacing of more than 100 km to about 25 km.
24 It is shown that Euro/Atlantic blocking is simulated overall more credibly at
25 higher resolution, i.e. in better agreement with a 50-year reference blocking
26 climatology created from the ERA-40 and ERA-Interim reanalyses. The im-
27 provement seen with resolution depends on the season and to some extent on
28 the model considered. Euro/Atlantic blocking is simulated more realistically
29 at higher resolution in winter, spring and autumn, and robustly so across the
30 model ensemble. The improvement in spring is larger than that in winter and
31 autumn. Summer blocking is found to be better simulated at higher resolution
32 by one model only, with little change seen in the other three models. The
33 representation of Pacific blocking is not found to systematically depend on
34 resolution. Despite the improvements seen with resolution, the 25-km mod-
35 els still exhibit large biases in Euro/Atlantic blocking. For example, three
36 of the four 25-km models underestimate winter northern European blocking
37 frequency by about one third. The resolution sensitivity and biases in the sim-
38 ulated blocking are shown to be in part associated with the mean-state biases
39 in the models' mid-latitude circulation.

40 **1. Introduction**

41 Blocking refers to the occurrence of quasi-stationary high-pressure systems at mid-latitudes and
42 can be described by a number of key characteristics (Barriopedro et al. 2010): blocking highs per-
43 sists for several days to weeks and often divert cyclones travelling in the stormtrack poleward or
44 equatorward (Rex 1950; Woollings et al. 2010; Zappa et al. 2014). Preferred regions of blocking
45 occurrence are the eastern sides of the Atlantic and Pacific Oceans. Blocks are observed through-
46 out the year with a peak occurrence in winter and spring (Tibaldi et al. 1994). The persistent
47 circulation during blocking episodes causes anomalous surface weather conditions and possibly
48 extreme events. Recent examples include the cold European winter 2009/2010 (Cattiaux et al.
49 2010) and the 2010 Russian heatwave (Barriopedro et al. 2011; Matsueda 2011; Otto et al. 2012).

50 Despite the lack of a single unified blocking theory, a number of detailed studies of the mecha-
51 nisms responsible for blocking formation and maintenance have been conducted. Croci-Maspoli
52 (2005) provide a brief overview of these studies and classify them into theories based on low-
53 frequency/planetary-scale and high-frequency/synoptic-scale dynamics. An example of the low-
54 frequency class is the study by Charney and DeVore (1979). Using a quasi-geostrophic zonal
55 channel model, it is shown in this study that there are two equilibrium states for the topographi-
56 cally driven disturbances of a zonal flow, a flow with a strong wave component (blocked situation)
57 and a flow with a stronger zonal component. In contrast to the low-frequency class, studies of
58 the high-frequency class include high-frequency activity such as transient eddies in the vicinity
59 of blocking formation and maintenance. These small-scale eddies are shown to be important for
60 the maintenance of blocking (Shutts 1983, 1986) and for sustaining low-frequency flow in general
61 (Kug and Jin 2009). Shutts (1983) show that the eddies transfer energy to the larger-scale split-jet

62 flow in a blocking situation and that the vorticity transport by the eddies can maintain blocking
63 patterns against advection by the mean flow.

64 Both coupled and atmosphere-only general circulation models (GCMs) tend to underestimate
65 the occurrence frequency and persistence of blocking events (D'Andrea et al. 1998; Boyle 2006;
66 Anstey et al. 2013; Masato et al. 2013). These biases are long-standing and the reasons for the
67 models' shortcomings are not fully understood. Several studies have shown that increasing the
68 horizontal resolution in an atmospheric model is beneficial for the representation of blocking in
69 the Northern (e.g., Matsueda et al. 2009; Jung et al. 2012) and Southern (Matsueda et al. 2010)
70 Hemisphere, consistent with the notion that the better representation of small-scale eddies and
71 orography (Berckmans et al. 2013) at higher resolution allow for a better simulation of blocking.
72 Other authors have emphasised the importance of improved physical parameterisations (Jung et al.
73 2010) and of vertical model resolution (Anstey et al. 2013).

74 Moreover, different arguments have been put forward to interpret the improvement in blocking
75 due to increased horizontal resolution. One possibility is that the simulation of blocking as a pro-
76 cess can be thought to be sensitive to model resolution. Another possibility is that it is mainly the
77 mean state of the model that is sensitive to resolution, and any improvement seen in the blocking
78 climatology is largely a reflection of the improvement of the mean state due to higher resolution
79 (Woollings 2010; Scaife et al. 2010). These two possibilities cannot be fully disentangled due to
80 the interaction between the mean state and eddies. However, some insight into the relevance of
81 the mean-state bias can be gained by correcting the mean bias in model data before the blocking
82 identification is applied (Scaife et al. 2010).

83 A robust assessment of blocking biases in models requires ensembles of multi-decadal simu-
84 lations because of the large variability of blocking on interannual and longer timescales. This
85 implies particular computational challenges when investigating the sensitivity to model resolution

86 since the required sampling statistics need to be accumulated at the highest desired resolution.
87 Therefore, investigations into the role of model resolution for blocking have relied either on the
88 ensembles of opportunity offered, for example, by the fifth phase of the Coupled Model Intercom-
89 parison Project (CMIP5; Anstey et al. 2013; Masato et al. 2013), or on the controlled increase of
90 resolution in individual GCMs (Matsueda et al. 2009; Jung et al. 2012; Berckmans et al. 2013).

91 Recent advances in computing power and investment in higher model resolution have enabled
92 several modelling centres to run atmospheric GCMs (AGCMs) at about 25 km grid spacing for the
93 simulation lengths/ensemble sizes required for the evaluation of blocking in these higher resolution
94 climate models. These advances allow the question of the resolution sensitivity of blocking to be
95 systematically revisited in a multi-model study. This study aims to use an ensemble of present-
96 day climate simulations from four AGCMs with about 25 km grid spacing at mid-latitudes to
97 (i) quantify biases in the representation of blocking throughout the year and (ii) to assess the
98 sensitivity of these biases to the model resolution. Furthermore, we follow the method suggested
99 by Scaife et al. (2010) to determine to what extent any blocking bias and resolution sensitivity are
100 associated with the mean-state bias of the models.

101 The outline of this paper is as follows: section 2 describes the blocking identification method,
102 the models and model experiments, and the reference reanalysis data against which we perform
103 evaluation. Section 3 illustrates the blocking climatology in reanalysis data and thereafter the
104 main results of this study regarding model performance and resolution sensitivity are presented in
105 section 4. Section 5 assesses the role of mean-state biases and the paper is concluded in section 6.

106 **2. Methods, models and data**

107 *a. Model ensemble and reanalyses*

108 This study is based on an ensemble comprising high-resolution AGCM simulations conducted
109 independently at four different modelling centres. The four models are the Community Atmo-
110 spheric Model (CAM5.1), the European Centre for Medium-Range Weather Forecasts (ECMWF)
111 Integrated Forecasting System (IFS), the Meteorological Research Institute model MRI-AGCM3.2
112 and the Met Office Hadley Centre Global Environmental Model (HadGEM3-GA3.0). Table 1
113 provides an overview of the four models and corresponding references, and Table 2 shows the
114 simulations that have been conducted with each model. For all four models, these experiments
115 are designed to test the sensitivity of the simulated climate to horizontal resolution only, i.e. re-
116 tuning at the different resolutions has been kept to a minimum (see, e.g., discussion in Demory
117 et al. 2014). Blocking climatologies are calculated for the full simulation period of each model
118 (Table 2) and evaluated against a 50-year reanalysis climatology (see also section 3).

119 The ECMWF Retrospective Analyses ERA-40 and ERA-Interim are used to evaluate the model
120 simulations. Additionally, blocking in these two reanalyses is compared with that in NASA's
121 Modern-ERA Retrospective Analysis for Research and Applications (MERRA) to assess the
122 agreement of different reanalyses on blocking climatologies. The three reanalyses are overviewed
123 in Table 3.

124 *b. Blocking identification*

125 We follow the blocking identification method used by Scherrer et al. (2006) using the absolute
126 geopotential height index (AGP). The AGP index is an extension of the blocking index used by
127 Tibaldi and Molteni (1990) to a two-dimensional map of blocking frequencies at every grid point.

128 In the AGP index, three conditions need to be fulfilled for a point at latitude ϕ_0 to be identified as
 129 blocked. The first condition is a reversal of the climatological equator-pole gradient of the 500-hPa
 130 geopotential height Z to the south of ϕ_0 :

$$\frac{Z(\phi_0) - Z(\phi_S)}{\phi_0 - \phi_S} > 0, \quad (1)$$

131 where ϕ_S is 15° south of ϕ_0 . The second condition requires westerly flow to the north of ϕ_0 :

$$\frac{Z(\phi_N) - Z(\phi_0)}{\phi_N - \phi_0} < -10 \text{ m}/^\circ\text{latitude}, \quad (2)$$

132 where ϕ_N is 15° north of ϕ_0 . The third condition is that the point is only considered blocked
 133 if the first two conditions are met for five consecutive days or more. As described by Scherrer
 134 et al. (2006), this persistence criterion is stricter than in some other studies (e.g., D'Andrea et al.
 135 1998; Doblas-Reyes et al. 2001) so that the AGP typically captures mature blocking states and
 136 AGP blocking frequencies are comparatively low. We apply the blocking index to daily instanta-
 137 neous 12 UTC geopotential height fields from models and reanalyses for all Northern Hemisphere
 138 grid points between 35°N and 75°N . All model and reanalysis fields are regridded to a common
 139 $1.875^\circ \times 1.25^\circ$ grid before the blocking identification is applied.

140 The AGP blocking index we use is a common (Scherrer et al. 2006; Anstey et al. 2013; Berck-
 141 mans et al. 2013), albeit to some extent subjective choice, and other indices have been suggested in
 142 the literature (see, e.g., Barriopedro et al. 2010, for an overview). An intercomparison of blocking
 143 identification methodologies is outside the scope of this study, but we recognise that the existence
 144 of different blocking indices may make it more difficult to directly compare between different
 145 studies. We refer to Scherrer et al. (2006) for a comparison of the AGP index with two other
 146 blocking indices. Additionally, the supplemental material shows examples of composites illustrat-
 147 ing how blocking is captured with the AGP index for different seasons and locations, and what the
 148 associated anomalies in surface pressure, temperature and precipitation are.

149 **3. Blocking in reanalyses**

150 In this preliminary section, we show how blocking is represented by the different reanalyses that
151 serve as the reference for the model simulations evaluated in section 4. Fig. 1 shows the clima-
152 tological blocking frequency from ERA-40 and ERA-Interim for the four seasons. During winter
153 (Fig. 1a), we reproduce the well-known (e.g., Anstey et al. 2013) distribution with blocking pre-
154 dominantly occurring in the Atlantic/European and Pacific sectors. Within the Atlantic/European
155 sector, preferred regions of blocking occurrence are over southeast Greenland, the North Sea, and
156 the Ural Mountains. In spring (Fig. 1b), two maxima of blocking frequency over Europe can be
157 seen to the west and north of the British Isles and to the east of the Baltic Sea. In summer, blocking
158 events are identified over a wide range of longitudes spanning Greenland, Eurasia and Alaska, and
159 there is no clear distinction between a region of Atlantic and Pacific blocking. Finally, during au-
160 tumn, the spatial distribution of blocking occurrence is similar to that in spring, but the frequency
161 is smaller than in spring throughout the Northern Hemisphere.

162 We use Fig. 1 to introduce some regions, outlined by the blue boxes, which will be used to
163 calculate area-averaged blocking statistics presented later in the paper. We refer to these regions
164 as Greenland (GL), Atlantic (ATL), Baltic (BAL), and Pacific (PAC). We also consider a North-
165 ern Europe (NEU) area which is the joint area of ATL and BAL and better corresponds to the
166 climatological spatial distribution of blocking frequency during winter.

167 Time series of the interannual variability of blocking frequency are shown in Fig. 2. It can be
168 seen that there is very close agreement between the ERA-40, ERA-Interim and MERRA reanalyses
169 products in Europe (Fig. 2a,b) and also close agreement in the PAC and GL regions (Fig. 2c,d)
170 where fewer in-situ observations are assimilated by the reanalyses. This close agreement is not
171 surprising since blocking anticyclones are slow-moving synoptic-scale systems that should be

172 captured by all of the reanalyses. This agreement also justifies using a concatenated dataset from
173 two reanalyses (Fig. 1) as the reference against which model simulations are evaluated.

174 Also evident from Fig. 2 is the large variability of blocking frequency at interannual and possibly
175 longer timescales. This large internal variability needs to be accounted for in the identification of
176 model biases. For the examples shown in Fig. 2, the coefficient of variation of the time series takes
177 values between about 0.5 and 1. A rough estimate of the minimal time series length n necessary to
178 identify a statistically significant difference in the mean blocking frequency can be obtained under
179 the simple assumptions of a z -test. A brief calculation shows that then $n = (1.96 c_{\text{var}}/\beta)^2$, where
180 $\beta = 1 - (\mu_1/\mu_2)$, $\mu_1 \leq \mu_2$, is the relative difference between the two time series means μ_1 and μ_2 ,
181 c_{var} is the coefficient of variation of time series 2, and 1.96 is the quantile of the standard Gaussian
182 corresponding to the customary confidence level of 95%. Taking $\beta = 0.2$, i.e. an underestimation
183 of the mean blocking frequency by 20%, yields $n = 24$ years for $c_{\text{var}} = 0.5$, and $n = 96$ years
184 for $c_{\text{var}} = 1$. These estimates show that the model ensemble used here (Table 2) is suitable for
185 identifying any large biases with respect to the 50-year reanalysis climatology shown in Fig. 1, as
186 well as large sensitivities to model resolution.

187 **4. Resolution sensitivity**

188 *a. Winter*

189 Fig. 3b–k shows the blocking frequency for the different models and resolutions in winter. The
190 reference reanalysis field already shown in Fig. 1a is repeated here for convenience in Fig. 3a.
191 All models represent the hemispheric-scale pattern of blocking frequency maxima in the At-
192 lantic/European and Pacific sectors, yet they exhibit biases in the details of the spatial distribution
193 and have a tendency to underestimate the blocking frequency at all resolutions. Two regions of

194 high blocking frequency over Greenland and in the region of the Ural Mountains are captured by
195 all of the models. In contrast, the low-resolution models (Fig. 3b,d,g,j) underestimate the blocking
196 frequency over the North Sea and show comparatively high blocking frequency over the south of
197 the British Isles and the Celtic Sea instead. This bias is reduced. in the high-resolution models
198 (Fig. 3c,f,i,k). The winter domain-mean blocking frequencies are shown in Fig. 4. The main result
199 of this figure is that three out of the four models (CAM5, IFS and UM) strongly underestimate the
200 winter blocking frequency. There is a slight improvement with resolution in the NEU domain for
201 the CAM5 and IFS models, yet considerable negative biases remain for most of the high-resolution
202 models: the NEU underestimation is 43% for CAM5, 28% for IFS, 9% for MRI and 30% for the
203 UM.

204 *b. Spring*

205 Figures 5 and 6 show that the resolution sensitivity is larger in spring (March–May) than in win-
206 ter. This is seen robustly across the ensemble: comparing the low-resolution results (Fig. 5b,d,g,j)
207 with the high-resolution results (Fig. 5c,f,i,k) in the Euro/Atlantic sector shows an increase in sim-
208 ulated blocking and a reduction of the bias with resolution. The domain-mean values shown in
209 Fig. 6 confirm that this increase is significant in three models (IFS, MRI, UM) in the NEU domain.
210 The spatial pattern of blocking frequency also agrees better with the reanalyses in the high resolu-
211 tion models. In the Euro/Atlantic sector, two distinct regions of high blocking frequency (i) over
212 Greenland and (ii) over an arc-shaped region stretching from west of Scotland to east of the Baltic
213 Sea are more markedly represented in the higher resolution models. Pacific blocking is captured
214 fairly well overall and at all resolutions, but underestimated by about 20% in the UM. Figures 5
215 and and 6 also show that, while there are clear limitations in how the models represent blocking

216 during the spring, the domain-mean biases are smaller than during winter. This is also seen in the
217 low-resolution models.

218 *c. Summer*

219 During summer (June–August, Fig. 7), there is no systematic sensitivity in the model biases to
220 resolution both in the Euro/Atlantic and Pacific sectors. The pattern of the biases differs some-
221 what between the models, however. In the IFS, the blocking frequency is underestimated nearly
222 everywhere and blocking is restricted to too high latitudes. In the MRI model, the geographical
223 distribution of blocking is in fairly close agreement with the reanalyses, but the blocking fre-
224 quency is underestimated in the PAC region. In the UM, the spatial distribution agrees closely
225 with the reanalysis blocking, but the blocking frequency is underestimated throughout the North-
226 ern Hemisphere. There is close agreement between the CAM5 blocking frequency pattern and
227 the reanalyses, and small-scale differences especially between the high-resolution CAM5 model
228 (Fig. 7k) and the reanalyses may be due to sampling variability for this single simulation. The
229 domain-mean blocking frequencies are shown in Fig. 8. The two regions with high reanalysis
230 summer blocking frequency are PAC and BAL. In the PAC region, blocking is considerably un-
231 derestimated by all four models, by between 58% (IFS T159) and 28% (CAM5 1°). The IFS and
232 UM also significantly underestimate blocking in the BAL region, both by approximately 50%,
233 whereas CAM5 and MRI agree fairly closely with the reanalysis in BAL.

234 *d. Autumn*

235 Finally, during autumn (September–November, Figures 9 and 10), the blocking frequency biases
236 are comparatively small for all resolutions and models, and accordingly the domain-mean biases
237 and resolution sensitivity are not significant for many of the regions/models. The most apparent

238 bias is the underestimation of PAC blocking in the CAM5 0.25° model (Figures 11k and 12d) by
239 about 60%.

240 *e. Pattern correspondence*

241 A quantitative assessment of the overall correspondence of the simulated and reanalysis block-
242 ing frequency patterns in the Atlantic/European sector is provided in Fig. 11. This figure shows
243 scatter plots of the root-mean-square-error (RMSE) and the spatial correlation of the model sim-
244 ulated blocking frequency pattern with the reanalysis pattern shown in Fig. 1. As the interannual
245 variability is better sampled in the ensemble-mean blocking-frequency pattern, the pertaining val-
246 ues of the RMSE (the spatial correlation) tend to be smaller (larger) than for individual ensemble
247 members. This fact needs to be considered for models where the ensemble size differs at the
248 different resolutions (Table 2).

249 The scatter plots in Fig. 11 confirm and in some cases show more clearly if there is a significant
250 improvement in the representation of Atlantic blocking with resolution. For example, for the UM
251 (Fig. 11d) an improvement with resolution is seen in the ensemble mean for all four seasons, yet
252 only during spring and summer this improvement is large compared with the typical difference
253 between ensemble members as shown by the fairly good separation of the “clouds” of points
254 corresponding to the low and high-resolution ensembles. This separation provides a qualitative
255 evaluation of the statistical significance of the differences in RMSE and correlation coefficient
256 between simulations at different resolutions. While all models show an improved representation of
257 blocking during spring, as was also shown in Fig. 5, they do not necessarily agree on improvements
258 in other seasons. For example, while there is a clear improvement during summer for the UM, the
259 MRI and IFS show improved Atlantic blocking in winter and little change or even a deterioration
260 during summer. Despite the biases remaining in the high resolution models, Fig. 11 shows an

261 overall improvement in the representation of blocking in the Atlantic sector with higher resolution.
262 Additionally, this figure also illustrates how a sufficient number of models/ensemble members are
263 needed in order to assess the sensitivity to resolution unequivocally.

264 Analogous scatter plots for the Pacific sector (not shown) do not reveal any systematic sensitivity
265 to resolution. This is consistent with results showing that the simulation of Pacific blocking is not
266 sensitive to horizontal resolution, for example in the CMIP5 ensemble (Anstey et al. 2013) and in
267 MRI AGCM3.1 (Matsueda et al. 2009). The sensitivity to resolution seen here for the European
268 region in winter, and possibly in spring, is also consistent with the findings that for CMIP5 models
269 (i) European blocking and storm-track biases are closely associated (Zappa et al. 2014) and (ii)
270 winter storm-track biases in the North Atlantic are reduced at higher resolution (Zappa et al. 2013).

271 **5. Blocking and mean-state biases**

272 In this section, we follow the approach of Scaife et al. (2010) to determine the degree to which
273 the blocking bias in the models is associated with their mean-state bias. We apply a correction to
274 the mean of the model 500-hPa geopotential height output and then re-calculate the blocking index
275 based on the bias-corrected height field. The procedure is illustrated in Fig. 12 for a single model
276 and grid point: the thin red line shows the daily climatological-mean geopotential height for the
277 UM at N96 resolution at this grid point. The bold red line is obtained by low-pass filtering this
278 data with a cutoff frequency at $(90 \text{ days})^{-1}$. The bold black line shows the same daily low-pass
279 filtered climatology for the reanalysis data, and the difference between the two bold lines defines
280 the model ‘mean’ bias on each day. Repeating this at each grid point defines the model bias at
281 each grid point and for each day of the year, and the model geopotential height is now corrected
282 for this bias before calculating the blocking climatology.

283 The middle column of Figure 13 (panels b,e,h,k) shows the winter blocking climatology ob-
284 tained after correcting the mean geopotential height to reanalysis in the lowest-resolution version
285 of the four models. This can be compared with the uncorrected blocking frequency and the refer-
286 ence reanalysis climatology shown in Fig. 3. It can be seen that the bias correction yields higher
287 blocking frequencies over north and west Europe in better agreement with the reanalysis (Fig. 3a)
288 than the uncorrected low-resolution models (Fig. 3b,d,g,j). There is some consistency between the
289 winter mean geopotential height bias of the four low-resolution models (shown in the left column
290 of Fig. 13, panels a,d,g,j) and the effect of bias correction on the blocking climatology. All models
291 have a low height bias over northwest Europe consistent with the general increase in blocking
292 frequency upon bias correction. For the MRI model whose height bias over northwest Europe is
293 fairly small, the effect of bias correction is fairly small as well.

294 Similarly to the uncorrected climatologies, however, the bias-corrected climatologies misplace
295 the North-Sea maximum of blocking occurrence southwestward over the south of the British Isles
296 and the Celtic Sea. This shows that the mean state bias, defined as described above, can only partly
297 account for the blocking biases seen in the low-resolution models.

298 We also show the resolution sensitivity in the winter mean 500 hPa geopotential height for the
299 four models on the right of Fig. 13, panels c,f,i,l. Over the Atlantic and Eurasia, the increase in
300 resolution largely reduces the biases in the low-resolution models. This is consistent with the slight
301 enhancement in Euro-Atlantic blocking seen with resolution. Yet again, the resolution sensitivity
302 of the mean geopotential height cannot fully explain the change in the blocking climatology with
303 resolution. For example, both the IFS and MRI models simulate higher occurrence of blocking
304 over the North Sea at higher resolution, while the geopotential height field in this area changes
305 strongly with resolution in the IFS model, but not so in the MRI model.

306 Moving on to spring (Fig. 14), we find that the blocking climatologies based on bias-corrected
307 height data agree overall better with the reanalyses (Fig. 5a) than the uncorrected climatologies of
308 the low-resolution models (Fig. 5b,d,g,j). As in winter, however, the association between mean-
309 state and blocking biases is far from perfect and varies strongly between the models: in the low-
310 resolution UM, for example, there is a pronounced negative height bias over central/northern Eu-
311 rope (Fig. 14g) and correcting for this height bias yields a strongly improved blocking climatology
312 and higher blocking frequency in the NEU area (Fig. 14h). Also, at high resolution this negative
313 height bias is smaller than at low resolution (Fig. 14i), which is consistent with the improvement
314 in the simulated blocking seen with resolution (Fig. 5g,h,i). In the low-resolution IFS model, there
315 is a negative height bias in the North-Atlantic/European midlatitudes and a positive bias in the
316 Arctic, particularly in the region of the Baffin Bay (Fig. 14a). Correcting for this bias has the
317 expected mixed effect on the blocking climatology, namely more frequent NEU blocking in better
318 agreement with the reanalyses and less frequent GL blocking in worse agreement with the reanaly-
319 ses (Fig. 14b, Fig. 5a,b). Also the change in the geopotential height bias with resolution (Fig. 14c)
320 is significant over the ATL area and very small over the BAL area, while the improvement in the
321 simulated blocking (Fig. 5c) can be seen in both areas and does not seem to be closely associated
322 with the mean-state bias.

323 In the summer, the low-resolution blocking biases appear to be more closely associated with the
324 mean-state biases than during winter and spring (Fig. 15 and Fig. 7): for example, all four models
325 have a positive height bias over the Gulf of Alaska whose correction yields more frequent PAC
326 blocking, in better agreement with the reanalyses. Also, with the exception of CAM5, the models
327 have a negative height bias in the BAL region and a positive bias over the Arctic, leading to more
328 frequent and more realistic blocking frequency when corrected. As discussed previously, however,
329 the improvement in the simulated blocking with higher resolution is fairly small. Even in the case

330 of the MRI model, whose mean-state bias is considerably smaller at high resolution (Fig. 15d,f),
331 there is only a slight improvement in the simulated blocking (Fig. 7d,e,f). Large biases remain
332 at the high resolution, showing that the reduction of a mean-state bias does not always imply a
333 similar reduction of the blocking bias.

334 As shown previously (Fig. 9), both the blocking biases and their resolution sensitivity are smaller
335 in autumn than in the other seasons. Here, we find that also the effect of bias-correcting the
336 geopotential height field has a fairly small, but beneficial, effect on the blocking climatology (not
337 shown). The height biases themselves and their resolution sensitivity, however, are of similar
338 magnitude to those in the other seasons.

339 **6. Conclusions**

340 We have evaluated the representation of Northern Hemisphere blocking in an ensemble of four
341 AGCMs whose atmospheric resolution is increased from more than 100 km to about 25 km hor-
342 izontal grid spacing. Simulations at this high resolution are still difficult and costly to carry out,
343 and few such simulations of sufficient length are available. We have analysed here, for the first
344 time, a multi-model ensemble of such simulations, and are therefore, for the first time, able to
345 document how robust the resolution sensitivity of blocking is at this scale. Overall, there is a clear
346 improvement in the simulated Euro/Atlantic blocking with resolution. At the same time, consid-
347 erable blocking frequency biases remain in the high-resolution models. For example, three of the
348 four high-resolution models (CAM5, IFS, UM) continue to underestimate European winter block-
349 ing frequency by about one third, and two models (IFS, UM) underestimate summer blocking
350 frequency in the Baltic area by about 50%.

351 The degree to which simulated Euro/Atlantic blocking improves with resolution depends on the
352 season, and in some cases on the particular model. The clearest improvement is seen in spring and

353 it is robust across the ensemble, eliminating most of the bias. Smaller improvements, which are
354 also robust across the ensemble, are seen in winter and autumn, whereby it should be noted that
355 the biases in autumn are smaller than those in the other seasons for all models, even at the low
356 resolutions. In summer, the resolution sensitivity is small and a significant improvement is only
357 found for the UM. In the Pacific, we do not find a systematic sensitivity to resolution, except for
358 CAM5 where there is some deterioration with increasing resolution in all seasons.

359 We have investigated the relationship between mean-state and blocking biases. This has been
360 done by correcting the model mean geopotential height field to the corresponding reanalysis value
361 while retaining the model geopotential height variability, and then recalculating the blocking cli-
362 matology. This separation is approximate due to the interaction between the mean state and eddies
363 but can still provide a qualitative idea of how closely mean-state and blocking biases are asso-
364 ciated with one another (Scaife et al. 2010). In agreement with previous studies (Scaife et al.
365 2010; Berckmans et al. 2013) we find that blocking biases are in part associated with mean-state
366 biases, and indeed we also find some improvement with resolution in the simulated mean state
367 of the extratropical atmosphere. Nonetheless, we also show that the agreement between mean-
368 state and blocking biases is far from perfect illustrating the need for further investigation into the
369 representation of blocking in climate models separate from biases in the mean circulation.

370 In summary, we show that AGCMs simulate atmospheric blocking more realistically as their grid
371 spacing is reduced to 25 km, yet considerable biases remain also at that resolution. Our results are
372 therefore consistent with previous studies pointing to the importance of model horizontal resolu-
373 tion, which are based on theoretical and numerical studies into the roles of small-scale eddies and
374 orography. At the same time, our results also support previous studies (Jung et al. 2010; Anstey
375 et al. 2013) showing that there are other factors than horizontal resolution limiting the represen-
376 tation of blocking in models. Future efforts should include research into (i) how further increases

377 in resolution and the simulation of coupled atmosphere-ocean processes (e.g., Minobe et al. 2008;
378 Hiron et al. 2015) might allow for a more credible simulation of blocking by climate models, the
379 reasons for (ii) the different resolution sensitivity for Atlantic and Pacific blocking and (iii) the sea-
380 sonality of the sensitivity to resolution over Europe, and (iv) how the model spread in the sensitivity
381 to resolution is related to the structure, physical parameterisations, and numerics of the individ-
382 ual models. The model experiments currently conducted in the European Horizon 2020 project
383 PRIMAVERA (PRocess-based climate sIMulation: AdVances in high-resolution modelling and
384 European climate Risk Assessment) and contributing to HighResMIP (Haarsma et al. 2016) will
385 offer the possibility to study some of these questions in a well-designed multi-model ensemble of
386 coupled (atmosphere, ocean, sea ice, land) climate models.

387 *Acknowledgments.* RS acknowledges NERC-Met Office JWCRP HRCM funding. PLV, MED
388 and JS acknowledge NCAS Climate contract R8/H12/83/001 for the High Resolution Climate
389 Modelling programme. PLV (UPSCALE PI) acknowledges the Willis Chair in Climate Sys-
390 tem Science and Climate Hazards that supports his research. The work of LCS was supported
391 by funding from the European Union’s Horizon 2020 research and innovation programme un-
392 der the IMPREX grant agreement No 641811. MJR and MSM were supported by the Joint UK
393 DECC/DEFRA Met Office Hadley Centre Climate Programme (GA01101). We thank the team of
394 model developers and infrastructure experts required to conduct the large UPSCALE simulation
395 campaign and acknowledge use of the MONSooN system, a collaborative facility supplied under
396 the JWCRP; the PRACE infrastructure; the Stuttgart HLRS supercomputing center, and the STFC
397 CEDA service for data storage and analysis using the JASMIN platform. The IFS results described
398 herein were obtained during the 2009–10 Athena Project, a computationally intensive project that
399 was carried out using the Athena supercomputer at the University of Tennessee’s National Institute

400 for Computational Sciences (NICS), under the auspices of the National Science Foundation (NSF).
401 Support provided by NICS and the NSF are gratefully acknowledged. The MRI model integra-
402 tions were performed using the Earth Simulator under the framework of the project “Projection
403 of the Change in Future Weather Extremes using Super-High-Resolution Atmospheric Models”
404 supported by the SOUSEI programs of the Ministry of Education, Culture, Sports, Science and
405 Technology (MEXT) of Japan. MFW was supported by the Regional and Global Climate Model-
406 ing Program of the Office of Biological and Environmental Research in the Department of Energy
407 Office of Science under contract number DE-AC02-05CH11231.

408 **References**

- 409 Anstey, J. A., and Coauthors, 2013: Multi-model analysis of Northern Hemisphere winter block-
410 ing: Model biases and the role of resolution. *J. Geophys. Res. Atmos.*, **118** (10), 3956–3971,
411 doi:10.1002/jgrd.50231.
- 412 Barriopedro, D., E. M. Fischer, J. Luterbacher, R. M. Trigo, and R. García-Herrera, 2011: The
413 hot summer of 2010: redrawing the temperature record map of Europe. *Science*, **332** (April),
414 220–224, doi:10.1126/science.1201224.
- 415 Barriopedro, D., R. García-Herrera, and R. M. Trigo, 2010: Application of blocking diagnosis
416 methods to General Circulation Models. Part I: a novel detection scheme. *Clim. Dyn.*, **35** (7-8),
417 1373–1391, doi:10.1007/s00382-010-0767-5.
- 418 Berckmans, J., T. Woollings, M.-E. Demory, P.-L. Vidale, and M. Roberts, 2013: Atmospheric
419 blocking in a high resolution climate model: influences of mean state, orography and eddy
420 forcing. *Atmos. Sci. Lett.*, **14** (1), 34–40, doi:10.1002/asl2.412.

- 421 Boyle, J. S., 2006: Upper level atmospheric stationary waves in the twentieth century climate
422 of the Intergovernmental Panel on Climate Change simulations. *J. Geophys. Res. Atmos.*, **111**,
423 doi:10.1029/2005JD006612.
- 424 Cattiaux, J., R. Vautard, C. Cassou, P. Yiou, V. Masson-Delmotte, and F. Codron, 2010: Winter
425 2010 in Europe: A cold extreme in a warming climate. *Geophys. Res. Lett.*, **37 (July)**, 1–6,
426 doi:10.1029/2010GL044613.
- 427 Charney, J. G., and J. G. DeVore, 1979: Multiple Flow Equilibria in the Atmosphere and Blocking.
428 *J. Atmos. Sci.*, **36 (7)**, 1205–1216, doi:10.1175/1520-0469(1979)036<1205:MFEITA>2.0.CO;2.
- 429 Croci-Maspoli, M., 2005: Climatological Investigations of Atmospheric Blocking -
430 A Dynamically-based Statistical Analysis. Ph.D. thesis, ETH Zürich, doi:10.3929/
431 ethz-a-005062167.
- 432 D'Andrea, F., and Coauthors, 1998: Northern Hemisphere atmospheric blocking as simulated by
433 15 atmospheric general circulation models in the period 1979-1988. *Clim. Dyn.*, **14 (6)**, 385–
434 407, doi:10.1007/s003820050230.
- 435 Dee, D. P., and Coauthors, 2011: The ERA-Interim reanalysis: configuration and performance of
436 the data assimilation system. *Q. J. R. Meteorol. Soc.*, **137 (656)**, 553–597, doi:10.1002/qj.828.
- 437 Demory, M.-E., P. L. Vidale, M. J. Roberts, P. Berrisford, J. Strachan, R. Schiemann, and M. S.
438 Mizielinski, 2014: The role of horizontal resolution in simulating drivers of the global hydro-
439 logical cycle. *Clim. Dyn.*, **42 (7-8)**, 2201–2225, doi:10.1007/s00382-013-1924-4.
- 440 Doblas-Reyes, F. J., M. A. Pastor, M. J. Casado, and M. Déqué, 2001: Wintertime westward-
441 traveling planetary-scale perturbations over the Euro-Atlantic region. *Clim. Dyn.*, **17 (10)**, 811–
442 824, doi:10.1007/s003820000146.

- 443 Donlon, C. J., M. Martin, J. Stark, J. Roberts-Jones, E. Fiedler, and W. Wimmer, 2012: The Oper-
444 ational Sea Surface Temperature and Sea Ice Analysis (OSTIA) system. *Remote Sens. Environ.*,
445 **116**, 140–158, doi:10.1016/j.rse.2010.10.017.
- 446 Gates, W. L., 1992: AMIP: The Atmospheric Model Intercomparison Project. *Bull. Am. Meteorol.*
447 *Soc.*, **73 (12)**, 1962–1970, doi:10.1175/1520-0477(1992)073<1962:ATAMIP>2.0.CO;2.
- 448 Haarsma, R. J., and Coauthors, 2016: High Resolution Model Intercomparison Project (High-
449 ResMIP). *Geosci. Model Dev. Discuss.*, (**April**), 1–35, doi:10.5194/gmd-2016-66.
- 450 Hirons, L. C., N. P. Klingaman, and S. J. Woolnough, 2015: MetUM-GOML1: a near-
451 globally coupled atmosphereocean-mixed-layer model. *Geosci. Model Dev.*, **8 (2)**, 363–379,
452 doi:10.5194/gmd-8-363-2015.
- 453 Jung, T., and Coauthors, 2010: The ECMWF model climate: Recent progress through improved
454 physical parametrizations. *Q. J. R. Meteorol. Soc.*, **136 (July)**, 1145–1160, doi:10.1002/qj.634.
- 455 Jung, T., and Coauthors, 2012: High-Resolution Global Climate Simulations with the ECMWF
456 Model in Project Athena: Experimental Design, Model Climate, and Seasonal Forecast Skill. *J.*
457 *Clim.*, **25 (9)**, 3155–3172, doi:10.1175/JCLI-D-11-00265.1.
- 458 Kinter, J. L., and Coauthors, 2013: Revolutionizing Climate Modeling with Project Athena: A
459 Multi-Institutional, International Collaboration. *Bull. Am. Meteorol. Soc.*, **94 (2)**, 231–245, doi:
460 10.1175/BAMS-D-11-00043.1.
- 461 Kug, J. S., and F. F. Jin, 2009: Left-hand rule for synoptic eddy feedback on low-frequency flow.
462 *Geophys. Res. Lett.*, **36 (5)**, 1–5, doi:10.1029/2008GL036435.
- 463 Masato, G., B. J. Hoskins, and T. Woollings, 2013: Winter and Summer Northern Hemisphere
464 Blocking in CMIP5 Models. *J. Clim.*, **26 (18)**, 7044–7059, doi:10.1175/JCLI-D-12-00466.1.

- 465 Matsueda, M., 2011: Predictability of Euro-Russian blocking in summer of 2010. *Geophys. Res.*
466 *Lett.*, **38 (6)**, 1–6, doi:10.1029/2010GL046557.
- 467 Matsueda, M., H. Endo, and R. Mizuta, 2010: Future change in Southern Hemisphere summertime
468 and wintertime atmospheric blockings simulated using a 20-km-mesh AGCM. *Geophys. Res.*
469 *Lett.*, **37 (2)**, L02 803, doi:10.1029/2009GL041758.
- 470 Matsueda, M., R. Mizuta, and S. Kusunoki, 2009: Future change in wintertime atmospheric block-
471 ing simulated using a 20-km-mesh atmospheric global circulation model. *J. Geophys. Res.*,
472 **114 (D12)**, D12 114, doi:10.1029/2009JD011919.
- 473 Minobe, S., A. Kuwano-Yoshida, N. Komori, S.-P. Xie, and R. J. Small, 2008: Influence of the
474 Gulf Stream on the troposphere. *Nature*, **452 (7184)**, 206–209, doi:10.1038/nature06690.
- 475 Mizuta, R., and Coauthors, 2012: Climate Simulations Using MRI-AGCM3.2 with 20-km Grid.
476 *J. Meteorol. Soc. Japan*, **90A**, 233–258, doi:10.2151/jmsj.2012-A12.
- 477 Neale, R. B., 2012: Description of the NCAR community atmosphere model (CAM 5.0). NCAR
478 Technical Note NCAR/TN-486+STR.
- 479 Otto, F. E. L., N. Massey, G. J. Van Oldenborgh, R. G. Jones, and M. R. Allen, 2012: Reconciling
480 two approaches to attribution of the 2010 Russian heat wave. *Geophys. Res. Lett.*, **39 (November**
481 **2011)**, 1–5, doi:10.1029/2011GL050422.
- 482 Rayner, N. A., D. E. Parker, E. B. Horton, C. K. Folland, L. V. Alexander, D. P. Rowell, E. C.
483 Kent, and A. Kaplan, 2003: Global analyses of sea surface temperature, sea ice, and night
484 marine air temperature since the late nineteenth century. *J. Geophys. Res.*, **108 (D14)**, 4407,
485 doi:10.1029/2002JD002670.

486 Rex, D. F., 1950: Blocking Action in the Middle Troposphere and its Effect upon Regional Cli-
487 mate. *Tellus*, **2** (4), 275–301, doi:10.1111/j.2153-3490.1950.tb00339.x.

488 Reynolds, R. W., N. A. Rayner, T. M. Smith, D. C. Stokes, and W. Wang, 2002: An im-
489 proved in situ and satellite SST analysis for climate. *J. Clim.*, **15** (13), 1609–1625, doi:
490 10.1175/1520-0442(2002)015<1609:AIISAS>2.0.CO;2.

491 Rienecker, M. M., and Coauthors, 2011: MERRA: NASAs Modern-Era Retrospective Analysis
492 for Research and Applications. *J. Clim.*, **24** (14), 3624–3648, doi:10.1175/JCLI-D-11-00015.1.

493 Scaife, A. A., T. Woollings, J. Knight, G. Martin, and T. Hinton, 2010: Atmospheric Blocking and
494 Mean Biases in Climate Models. *J. Clim.*, **23** (23), 6143–6152, doi:10.1175/2010JCLI3728.1.

495 Scherrer, S. C., M. Croci-Maspoli, C. Schwierz, and C. Appenzeller, 2006: Two-dimensional
496 indices of atmospheric blocking and their statistical relationship with winter climate patterns in
497 the Euro-Atlantic region. *Int. J. Climatol.*, **26** (2), 233–249, doi:10.1002/joc.1250.

498 Shutts, G. J., 1983: The propagation of eddies in diffuent jetstreams : eddy vorticity forcing of '
499 blocking ' flow fields. *Q. J. R. Meteorol. Soc.*, (109), 737–761, doi:10.1002/qj.49710946204.

500 Shutts, G. J., 1986: A Case Study of Eddy Forcing During an Atlantic Blocking Episode. *Anoma-*
501 *lous Atmos. Flows Blocking*, R. B. Barry Saltzman, and A. C. Wiin-Nielsen, Eds., Advances in
502 Geophysics, Vol. 29, Elsevier, 135–162, doi:10.1016/S0065-2687(08)60037-0.

503 Tibaldi, S., and F. Molteni, 1990: On the operational predictability of blocking. *Tellus A*, **42** (3),
504 343–365, doi:10.3402/tellusa.v42i3.11882.

505 Tibaldi, S., E. Tosi, A. Navarra, and L. Pedulli, 1994: Northern and Southern Hemisphere
506 Seasonal Variability of Blocking Frequency and Predictability. 1971–2003 pp., doi:10.1175/
507 1520-0493(1994)122<1971:NASHSV>2.0.CO;2.

- 508 Uppala, S. M., and Coauthors, 2005: The ERA-40 re-analysis. *Q. J. R. Meteorol. Soc.*, **131** (612),
509 2961–3012, doi:10.1256/qj.04.176.
- 510 Walters, D. N., and Coauthors, 2011: The Met Office Unified Model Global Atmosphere 3.0/3.1
511 and JULES Global Land 3.0/3.1 configurations. *Geosci. Model Dev.*, **4** (4), 919–941, doi:10.
512 5194/gmd-4-919-2011.
- 513 Woollings, T., 2010: Dynamical influences on European climate: an uncertain future. *Philos.*
514 *Trans. A. Math. Phys. Eng. Sci.*, **368**, 3733–3756, doi:10.1098/rsta.2010.0040.
- 515 Woollings, T., A. Hannachi, and B. Hoskins, 2010: Variability of the North Atlantic eddy-driven
516 jet stream. *Q. J. R. Meteorol. Soc.*, **136** (649), 856–868, doi:10.1002/qj.625.
- 517 Zappa, G., G. Masato, L. Shaffrey, T. Woollings, and K. Hodges, 2014: Linking Northern Hemi-
518 sphere blocking and storm track biases in the CMIP5 climate models. *Geophys. Res. Lett.*,
519 **41** (October 2013), 135–139, doi:10.1002/2013GL058480.
- 520 Zappa, G., L. C. Shaffrey, and K. I. Hodges, 2013: The Ability of CMIP5 Models to Sim-
521 ulate North Atlantic Extratropical Cyclones*. *J. Clim.*, **26** (15), 5379–5396, doi:10.1175/
522 JCLI-D-12-00501.1.

523 **LIST OF TABLES**

524 **Table 1.** AGCMs used in this study. 27

525 **Table 2.** Model experiments. Grid spacings are given at 50°N for CAM5 and UM
526 (square root of grid-box area and zonal × meridional spacing in parenthesis).
527 IFS and MRI are spectral models. The sea surface temperature (SST) forcing
528 data sets are monthly Atmospheric Model Intercomparison Project I (AMIP I,
529 Gates 1992), three different SST products for the Athena IFS simulations (see
530 Jung et al. 2012, for details), monthly HadISST1 (Rayner et al. 2003), and daily
531 OSTIA forcing (Donlon et al. 2012). 28

532 **Table 3.** Reanalyses used in this study. The grid spacing is given at 50°N for MERRA
533 (square root of grid-box area and zonal × meridional spacing in parenthesis). . . . 29

TABLE 1. AGCMs used in this study.

Acronym	Model	Centre	Vertical levels	References
CAM5	CAM5.1	National Center for Atmospheric Research (USA)	30	Neale (2012)
IFS	IFS (Athena)	European Centre for Medium-Range Weather Forecasts (United Kingdom)	91	Jung et al. (2012), Kinter et al. (2013)
MRI	MRI-AGCM3.2	Meteorological Research Institute (Japan)	64	Mizuta et al. (2012)
UM	HadGEM3-GA3.0	Met Office Hadley Centre (United Kingdom)	85	Walters et al. (2011)

534 TABLE 2. Model experiments. Grid spacings are given at 50°N for CAM5 and UM (square root of grid-
535 box area and zonal × meridional spacing in parenthesis). IFS and MRI are spectral models. The sea surface
536 temperature (SST) forcing data sets are monthly Atmospheric Model Intercomparison Project I (AMIP I, Gates
537 1992), three different SST products for the Athena IFS simulations (see Jung et al. 2012, for details), monthly
538 HadISST1 (Rayner et al. 2003), and daily OSTIA forcing (Donlon et al. 2012).

Model	Resolution	Grid spacing (km)	Ensemble (size × years)	Period	SST forcing
CAM5	1.3° × 0.9°	96 (93 × 100)	3 × 27	1979–2005	AMIP I
CAM5	0.31° × 0.23°	24 (22 × 26)	1 × 27	1979–2005	AMIP I
IFS	T159	126	1 × 46	1962–2007	Athena
IFS	T1279	16	1 × 46	1962–2007	Athena
MRI	T95	208	4 × 25	1979–2003	HadISST1
MRI	T319	63	4 × 25	1979–2003	HadISST1
MRI	T959	21	2 × 25	1979–2003	HadISST1
UM	N96	136 (134 × 139)	5 × 26	1986–2011	OSTIA
UM	N216	61 (60 × 62)	3 × 26	1986–2011	OSTIA
UM	N512	26 (25 × 26)	5 × 26	1986–2011	OSTIA

539 TABLE 3. Reanalyses used in this study. The grid spacing is given at 50°N for MERRA (square root of
 540 grid-box area and zonal × meridional spacing in parenthesis).

Reanalysis	Resolution	Grid spacing (km)	Period	SST forcing	Reference
ERA-40	T159	126	1958–2001	HadISST1 (Rayner et al. 2003), Reynolds et al. (2002)	Uppala et al. (2005)
ERA-Interim	T255	79	1979 to present	(several, see reference)	Dee et al. (2011)
MERRA	$2\frac{1}{3}^\circ \times \frac{1}{2}^\circ$	51 (48 × 56)	1979 to present	Reynolds et al. (2002)	Rienecker et al. (2011)

LIST OF FIGURES

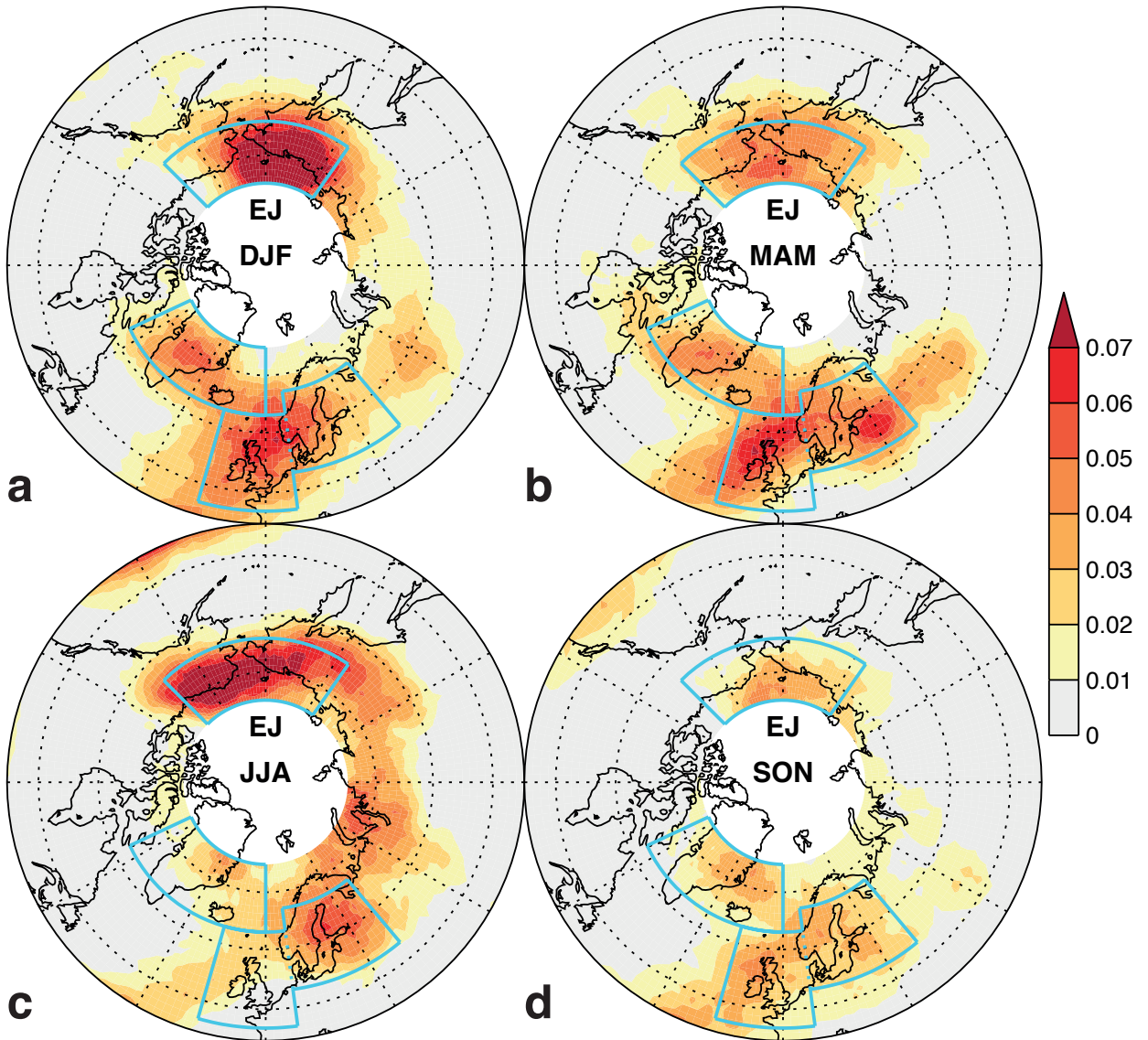
541		
542	Fig. 1.	Climatological-mean reanalysis blocking frequency (fraction of blocked days) based on concatenating ERA-40 (1962–1978) and ERA-Interim (1979–2011) for (a) December–February, (b) March–May, (c) June–August, and (d) September–November. The lightblue lines show five regions: ATL (–16–7.5°E, 47–63°N), BAL (7.5–40°E, 53–67°N), PAC (145–225°E, 64–75°N), GL (295–0°E, 63–75°N), and NEU which is the joint area of ATL and BAL. 32
543		
544		
545		
546		
547	Fig. 2.	Examples of 50-year time series of blocking frequency, spatially averaged over the regions shown in Fig. 1, and for boreal winter or summer. Symbols show ERA-Interim (triangles, 1979–2011) and MERRA (crosses, 1979–2011), and ERA-40 (circles, 1962–2001). The solid line shows the concatenated reference time series composed of ERA-40 (1962–1978) and ERA-Interim (1979–2011). The inset shows the mean (μ), standard deviation (σ), and coefficient of variation (c_{var}) of this reference time series. 33
548		
549		
550		
551		
552		
553	Fig. 3.	December–February climatological and ensemble-mean blocking frequency (fraction of blocked days). (a) ERA reanalyses as in Fig 1. (b) IFS at T159 resolution, (c) IFS at T1279, (d) MRI at TL95, (e) MRI at T319, (f) MRI at T959, (g) UM at N96, (h) UM at N216, (i) UM at N512, (j) CAM5 at $1.3^\circ \times 0.9^\circ$, (k) CAM5 at $0.31^\circ \times 0.23^\circ$ 35
554		
555		
556		
557	Fig. 4.	December–February climatological and ensemble-mean blocking frequency for regions defined in Fig. 1. ERA-40/ERA-Interim reanalysis values (as in Fig. 1) are shown for 1962–2011 on the left in terms of the mean (black dot and horizontal dashed line) \pm the ensemble mean of one standard deviation of interannual variability (grey bar). Reanalysis blocking frequencies are also shown for each of the simulation periods of the four models. Coloured green/blue dots and bars show the same information for the four models at different resolutions. Triangles indicate significant test results for differences, e.g. the downward triangles in (a) for CAM5 1° and 0.25° indicate that the blocking frequency in these two models is significantly smaller than in the reanalysis. In the same way, coloured triangles show significant differences between different resolutions of a model. The test employed is a t -test comparing the mean of two samples composed of the yearly ensemble-mean blocking frequencies of the two datasets at hand. 37
558		
559		
560		
561		
562		
563		
564		
565		
566		
567		
568		
569	Fig. 5.	As Fig. 3 but for spring (March–May). 38
570	Fig. 6.	As Fig. 4 but for spring (March–May). 39
571	Fig. 7.	As Fig. 3 but for summer (June–August). 40
572	Fig. 8.	As Fig. 4 but for summer (June–August). 41
573	Fig. 9.	As Fig. 3 but for autumn (September–November). 42
574	Fig. 10.	As Fig. 4 but for autumn (September–November). 43
575	Fig. 11.	Blocking frequency root-mean-square error and spatial correlation with respect to the reanalysis blocking frequency field shown in Fig. 1 for the Atlantic/European sector (80°W – 80°E , 45 – 75°N). Panels (a–d) are for the four different models, small symbols correspond to ensemble members and bold symbols to the ensemble mean (see Table 2). 44
576		
577		
578		
579	Fig. 12.	Illustration of bias correction of the 500-hPa geopotential height field for a single grid box at 0°E 56.25°N and for the UM at N96 resolution (red) with respect to ERA-40/ERA-Interim reanalysis data as in Fig. 1 (black). Thin lines show the daily climatological-mean value,
580		
581		

582 and bold lines show the daily climatological-mean value after lowpass-filtering with a cutoff
 583 frequency at $(90 \text{ days})^{-1}$. Vertical dashed lines show the canonical northern-hemisphere
 584 seasons. 45

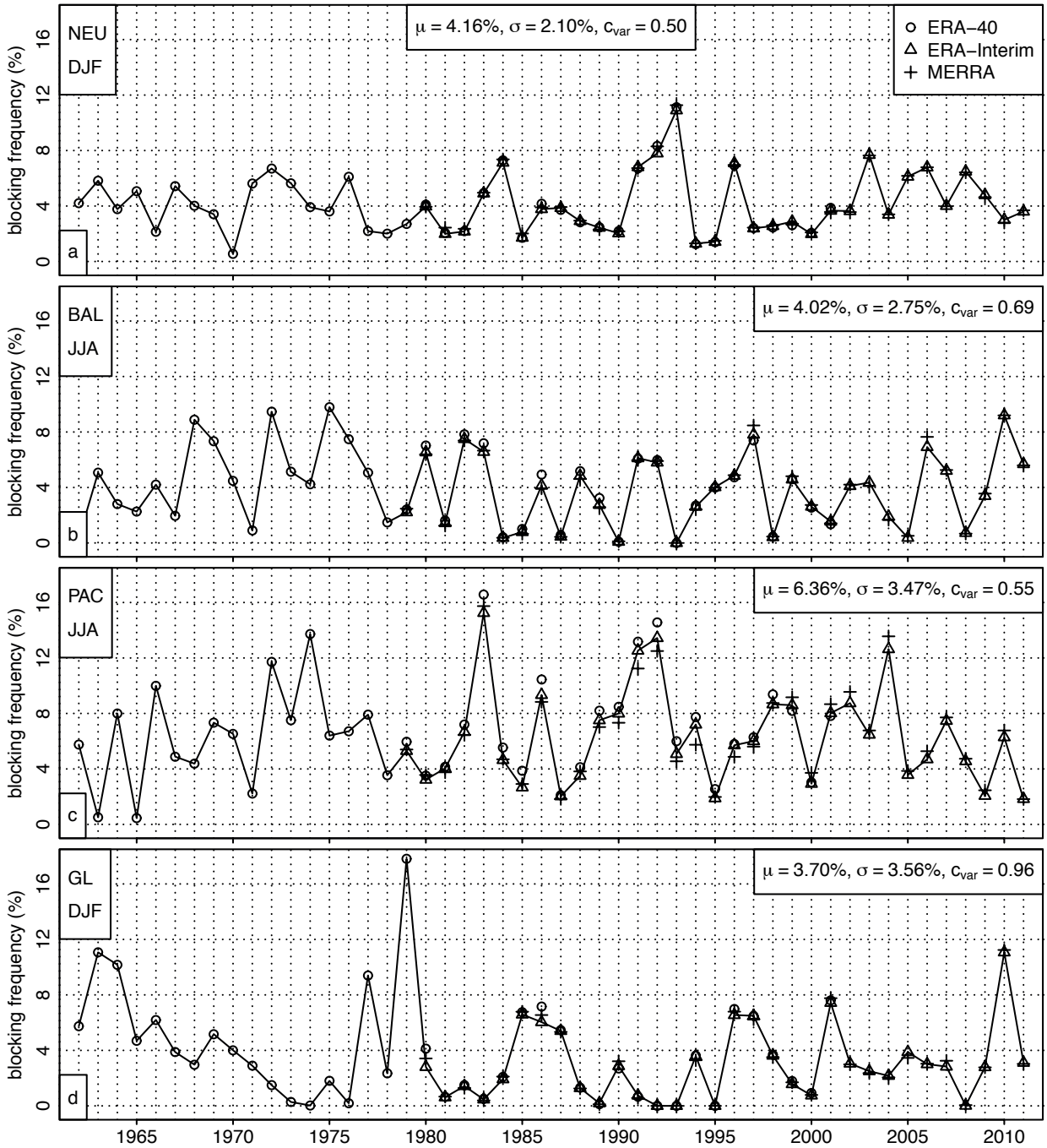
585 **Fig. 13.** December–February (a,d,g,j) 500-hPa geopotential height bias (m), (b,e,h,k) blocking fre-
 586 quency calculated from bias-corrected geopotential height data for lowest resolution model
 587 (e.g., N96 for the UM), (c,f,i,l) 500-hPa geopotential height difference (m) for highest min-
 588 us lowest resolution model (e.g., N512 - N96 for the UM). The models are (a,b,c) IFS,
 589 (d,e,f) MRI, (g,h,i) UM and (j,k,l) CAM5. Grey lines enclose areas of statistically signif-
 590 icant geopotential height differences. Stippling shows regions where correcting the height
 591 bias reduces the blocking bias (b,e,h,k), and where the height bias decreases with the reso-
 592 lution increase (c,f,i,l). 47

593 **Fig. 14.** As Fig. 13 but for spring (March–May). 48

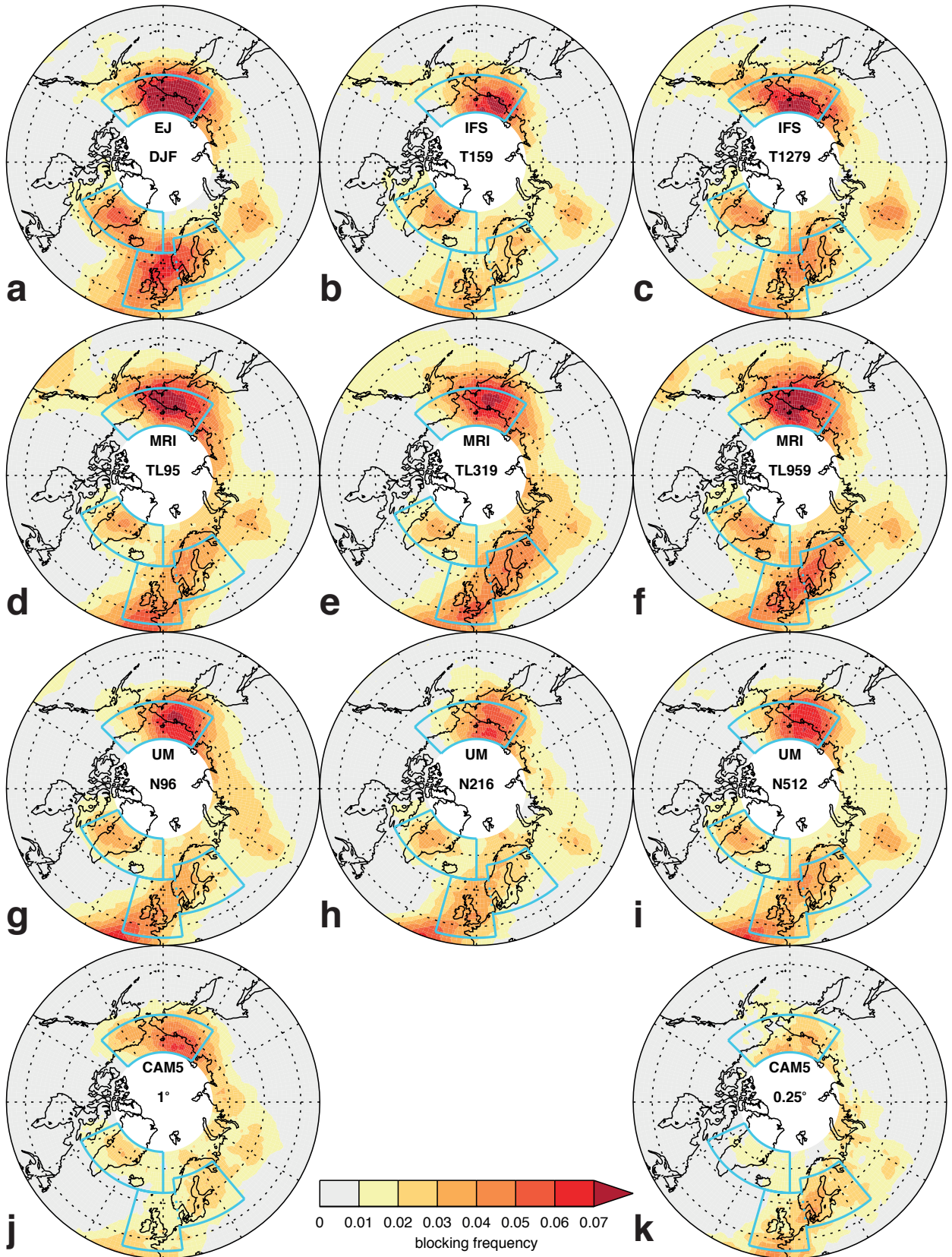
594 **Fig. 15.** As Fig. 13 but for summer (June–August). 49



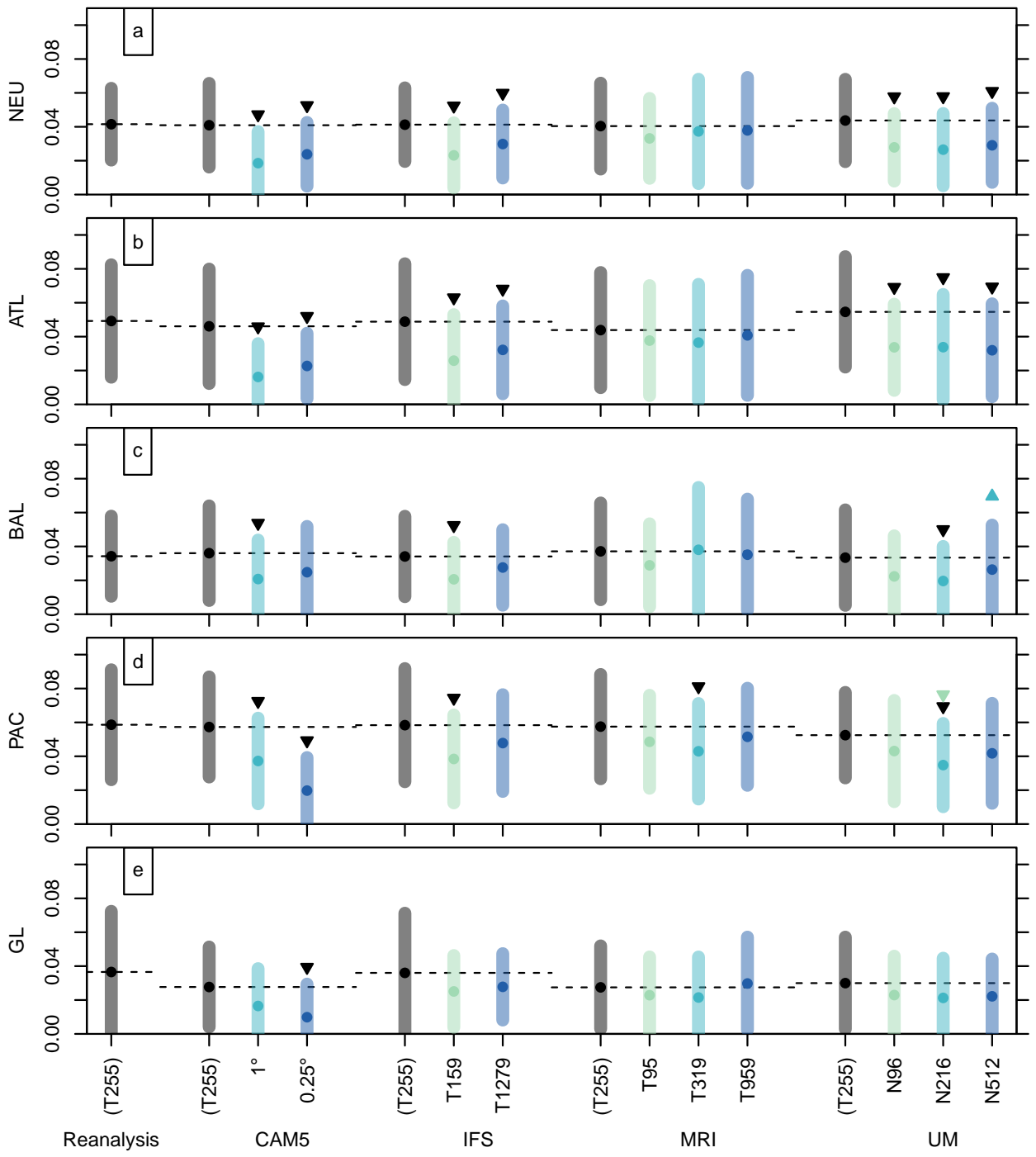
595 FIG. 1. Climatological-mean reanalysis blocking frequency (fraction of blocked days) based on concatenating
 596 ERA-40 (1962–1978) and ERA-Interim (1979–2011) for (a) December–February, (b) March–May, (c) June–
 597 August, and (d) September–November. The lightblue lines show five regions: ATL ($-16\text{--}7.5^\circ\text{E}$, $47\text{--}63^\circ\text{N}$), BAL
 598 ($7.5\text{--}40^\circ\text{E}$, $53\text{--}67^\circ\text{N}$), PAC ($145\text{--}225^\circ\text{E}$, $64\text{--}75^\circ\text{N}$), GL ($295\text{--}0^\circ\text{E}$, $63\text{--}75^\circ\text{N}$), and NEU which is the joint area
 599 of ATL and BAL.



600 FIG. 2. Examples of 50-year time series of blocking frequency, spatially averaged over the regions shown
 601 in Fig. 1, and for boreal winter or summer. Symbols show ERA-Interim (triangles, 1979–2011) and MERRA
 602 (crosses, 1979–2011), and ERA-40 (circles, 1962–2001). The solid line shows the concatenated reference time
 603 series composed of ERA-40 (1962–1978) and ERA-Interim (1979–2011). The inset shows the mean (μ), stan-
 604 dard deviation (σ), and coefficient of variation (c_{var}) of this reference time series.



605 FIG. 3. December–February climatological and ensemble-mean blocking frequency (fraction of blocked
606 days). (a) ERA reanalyses as in Fig 1. (b) IFS at T159 resolution, (c) IFS at T1279, (d) MRI at TL95, (e)
607 MRI at T319, (f) MRI at T959, (g) UM at N96, (h) UM at N216, (i) UM at N512, (j) CAM5 at $1.3^\circ \times 0.9^\circ$, (k)
608 CAM5 at $0.31^\circ \times 0.23^\circ$.



609 FIG. 4. December–February climatological and ensemble-mean blocking frequency for regions defined in
610 Fig. 1. ERA-40/ERA-Interim reanalysis values (as in Fig. 1) are shown for 1962–2011 on the left in terms of
611 the mean (black dot and horizontal dashed line) \pm the ensemble mean of one standard deviation of interannual
612 variability (grey bar). Reanalysis blocking frequencies are also shown for each of the simulation periods of the
613 four models. Coloured green/blue dots and bars show the same information for the four models at different
614 resolutions. Triangles indicate significant test results for differences, e.g. the downward triangles in (a) for
615 CAM5 1° and 0.25° indicate that the blocking frequency in these two models is significantly smaller than in the
616 reanalysis. In the same way, coloured triangles show significant differences between different resolutions of a
617 model. The test employed is a *t*-test comparing the mean of two samples composed of the yearly ensemble-mean
618 blocking frequencies of the two datasets at hand.

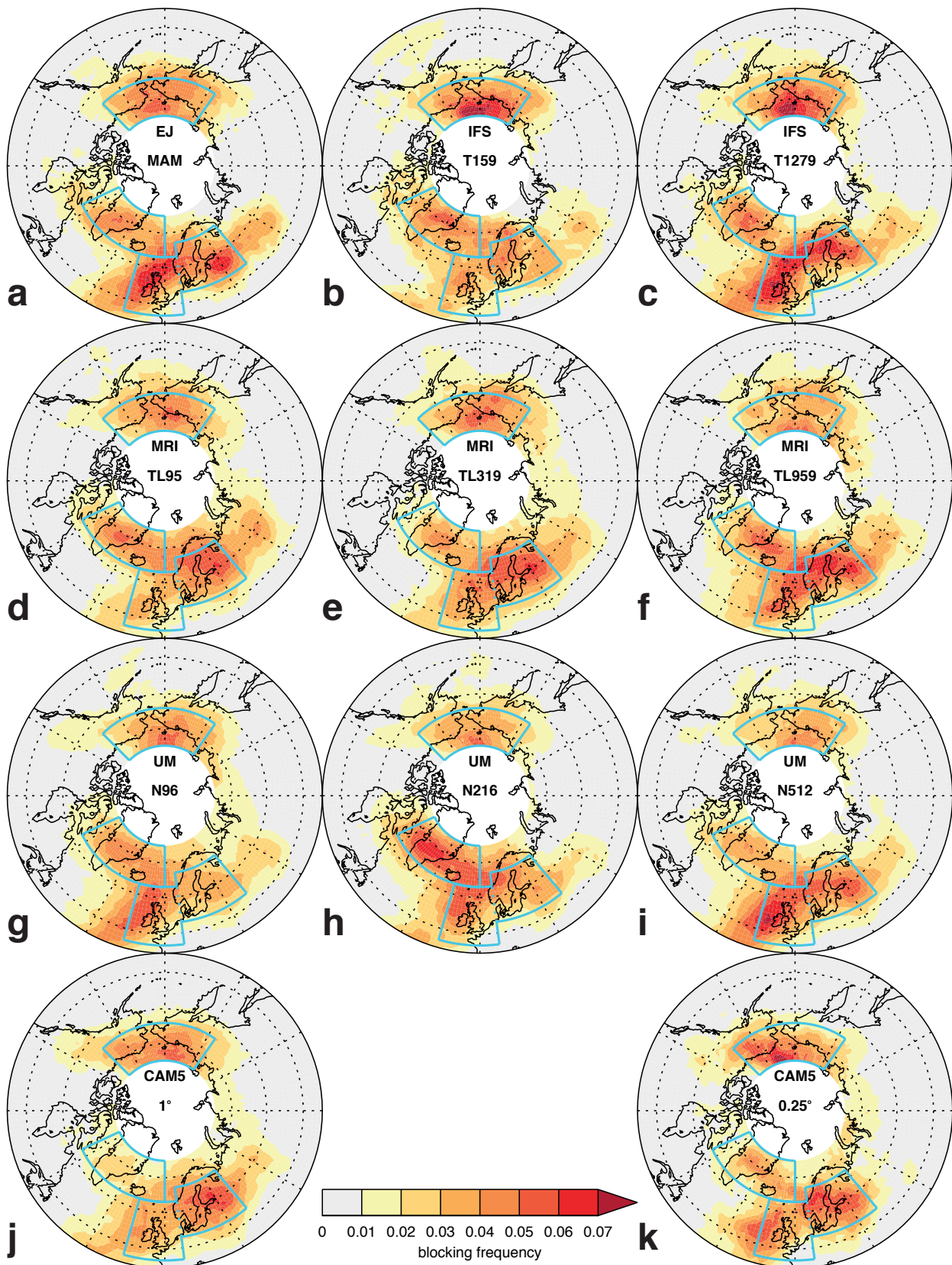


FIG. 5. As Fig. 3 but for spring (March–May).

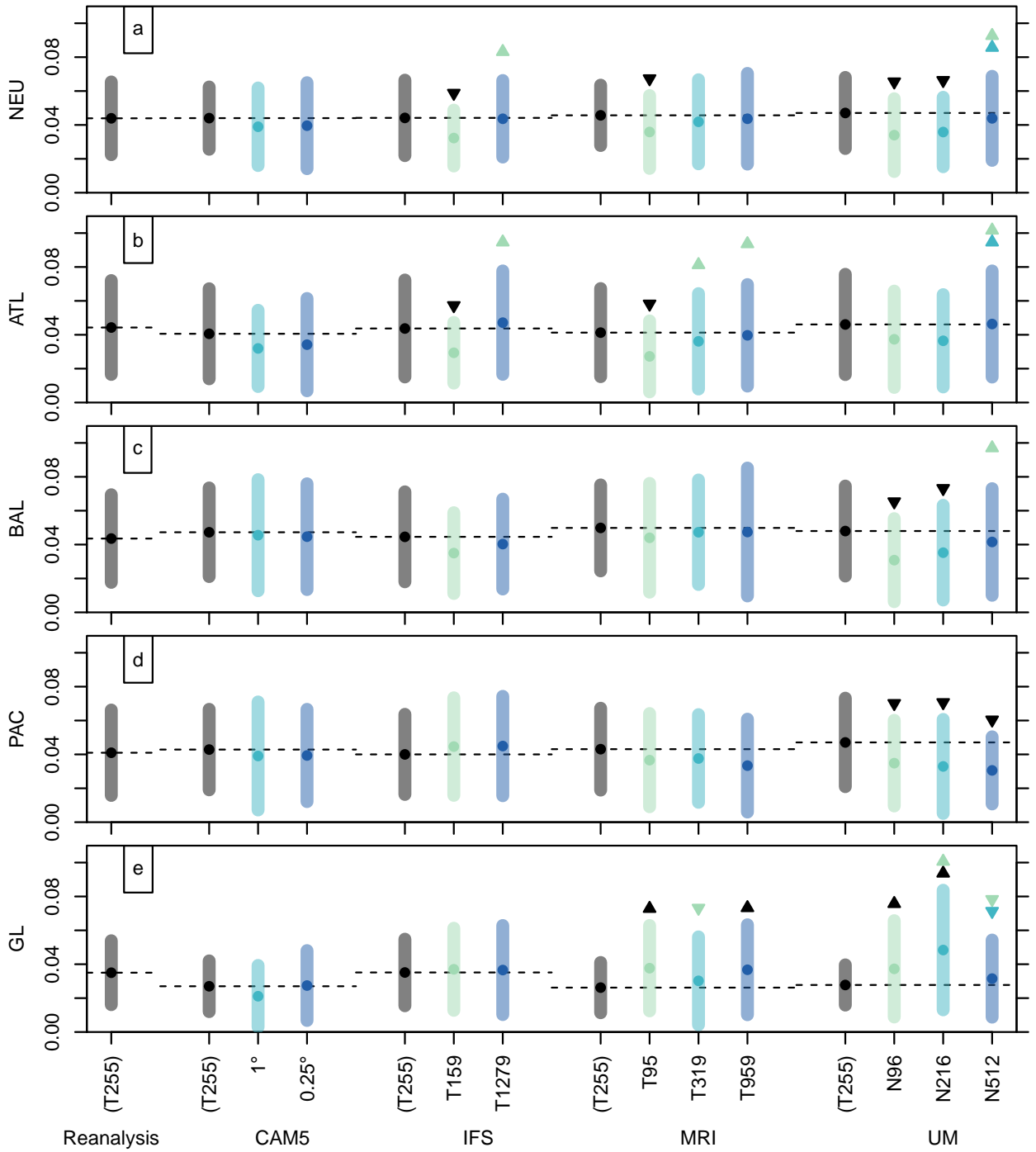


FIG. 6. As Fig. 4 but for spring (March–May).

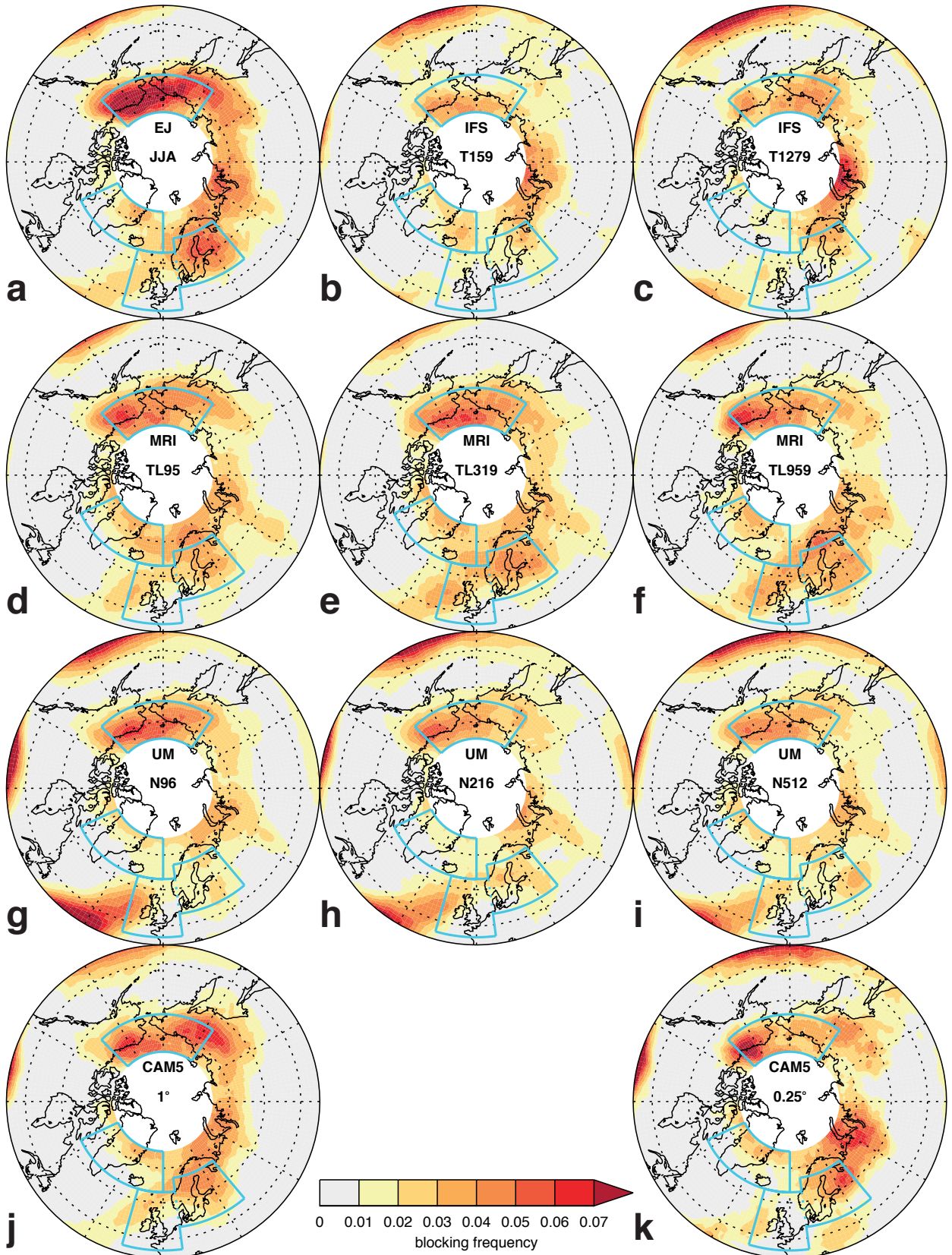


FIG. 7. As Fig. 3 but for summer (June–August).

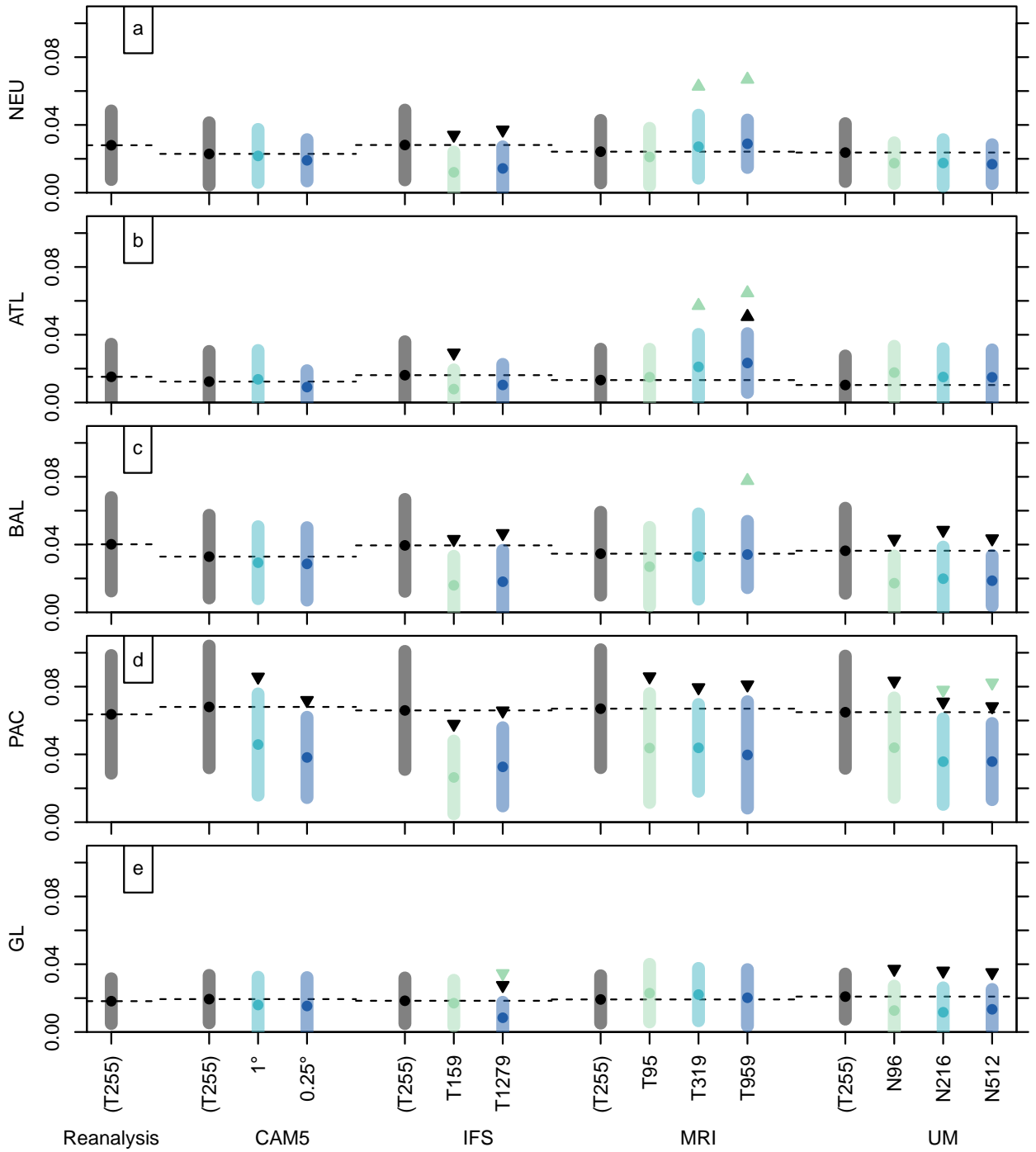


FIG. 8. As Fig. 4 but for summer (June–August).

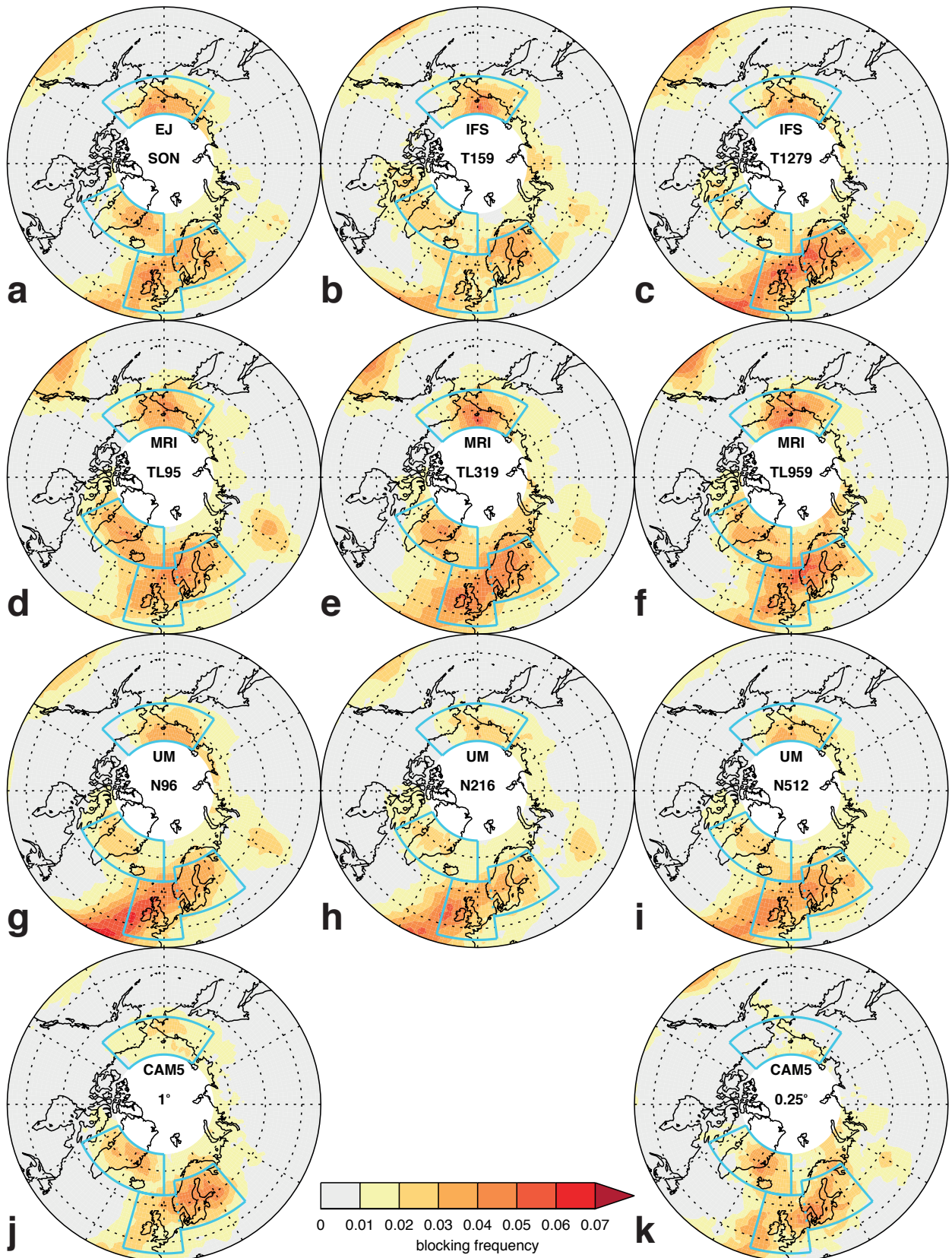


FIG. 9. As Fig. 3 but for autumn (September–November).

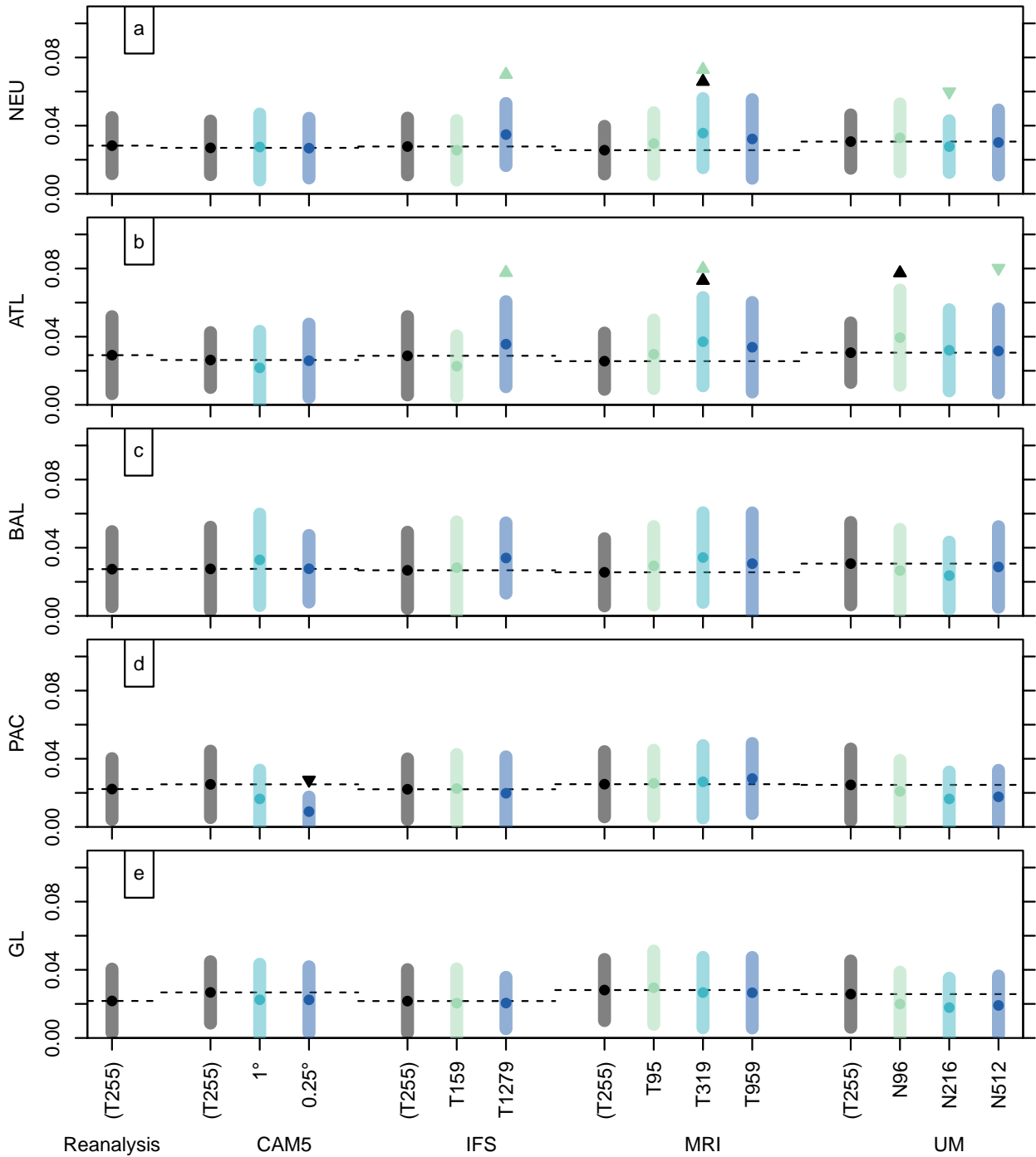
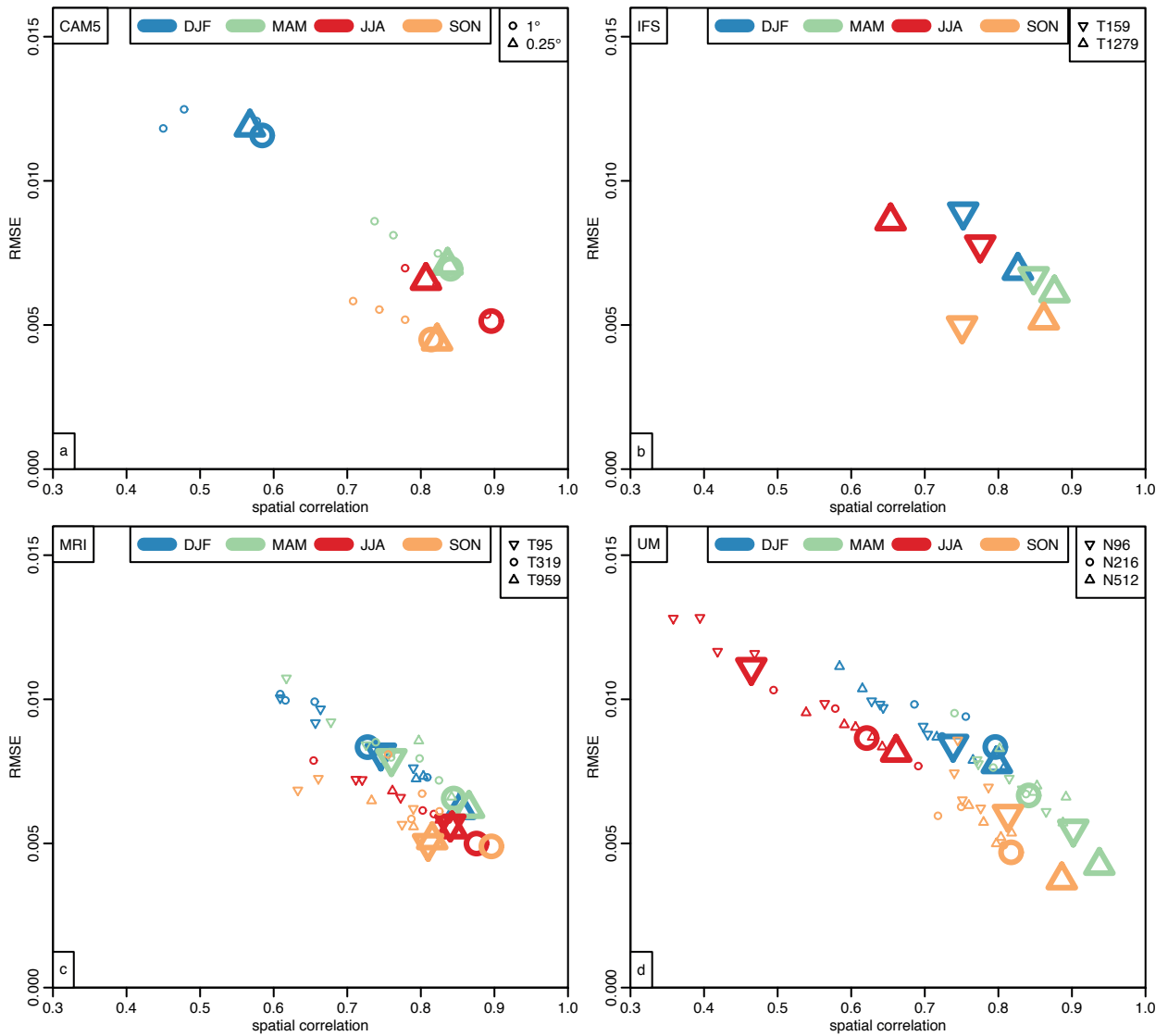
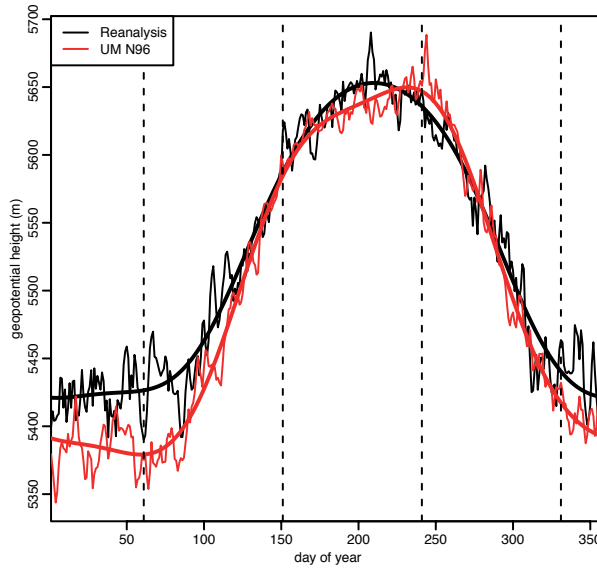


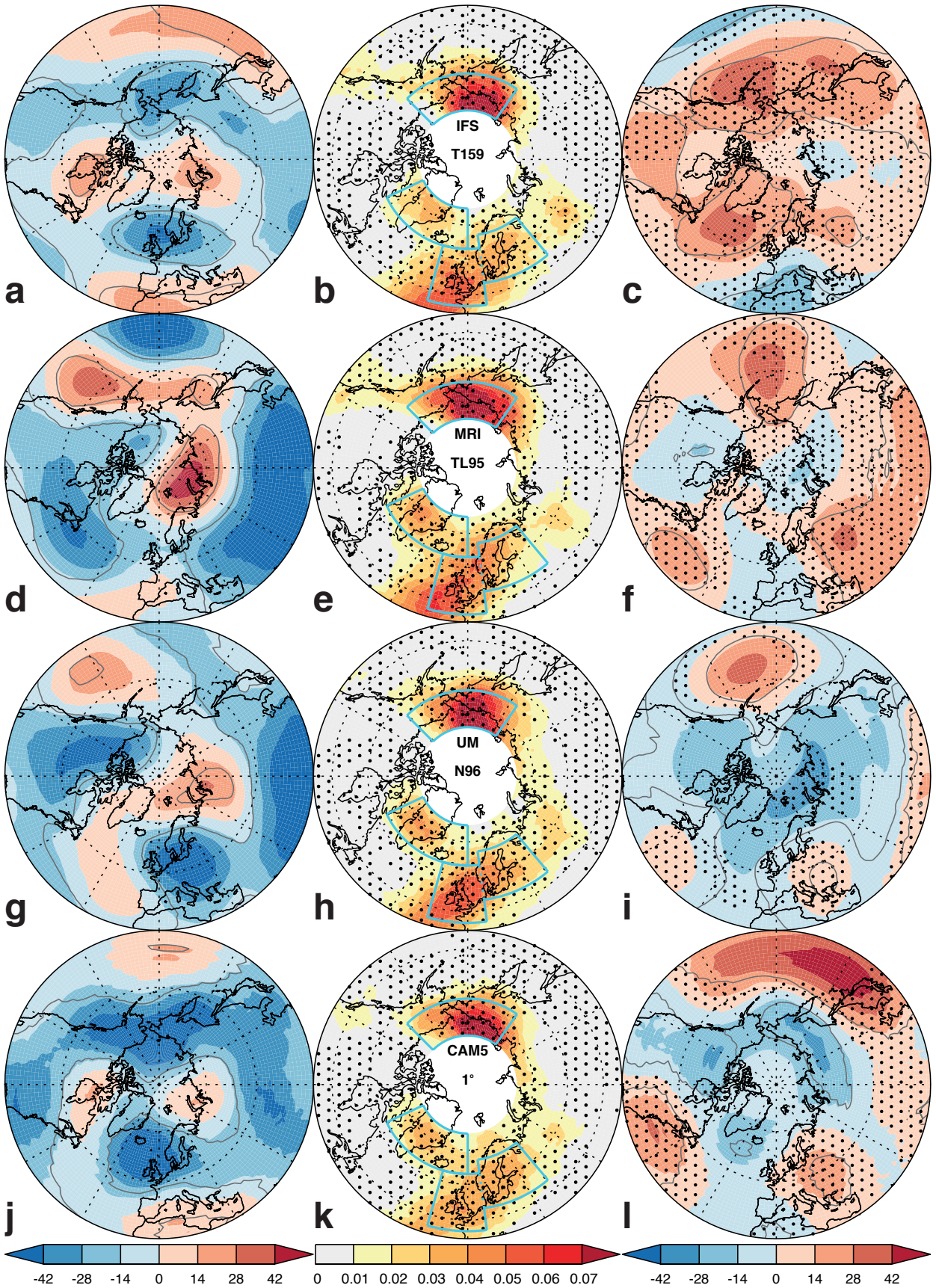
FIG. 10. As Fig. 4 but for autumn (September–November).



619 FIG. 11. Blocking frequency root-mean-square error and spatial correlation with respect to the reanalysis
 620 blocking frequency field shown in Fig. 1 for the Atlantic/European sector (80°W–80°E, 45–75°N). Panels (a–
 621 d) are for the four different models, small symbols correspond to ensemble members and bold symbols to the
 622 ensemble mean (see Table 2).



623 FIG. 12. Illustration of bias correction of the 500-hPa geopotential height field for a single grid box at 0°E
 624 56.25°N and for the UM at N96 resolution (red) with respect to ERA-40/ERA-Interim reanalysis data as in Fig. 1
 625 (black). Thin lines show the daily climatological-mean value, and bold lines show the daily climatological-mean
 626 value after lowpass-filtering with a cutoff frequency at $(90 \text{ days})^{-1}$. Vertical dashed lines show the canonical
 627 northern-hemisphere seasons.



628 FIG. 13. December–February (a,d,g,j) 500-hPa geopotential height bias (m), (b,e,h,k) blocking frequency
629 calculated from bias-corrected geopotential height data for lowest resolution model (e.g., N96 for the UM),
630 (c,f,i,l) 500-hPa geopotential height difference (m) for highest minus lowest resolution model (e.g., N512 - N96
631 for the UM). The models are (a,b,c) IFS, (d,e,f) MRI, (g,h,i) UM and (j,k,l) CAM5. Grey lines enclose areas of
632 statistically significant geopotential height differences. Stippling shows regions where correcting the height bias
633 reduces the blocking bias (b,e,h,k), and where the height bias decreases with the resolution increase (c,f,i,l).

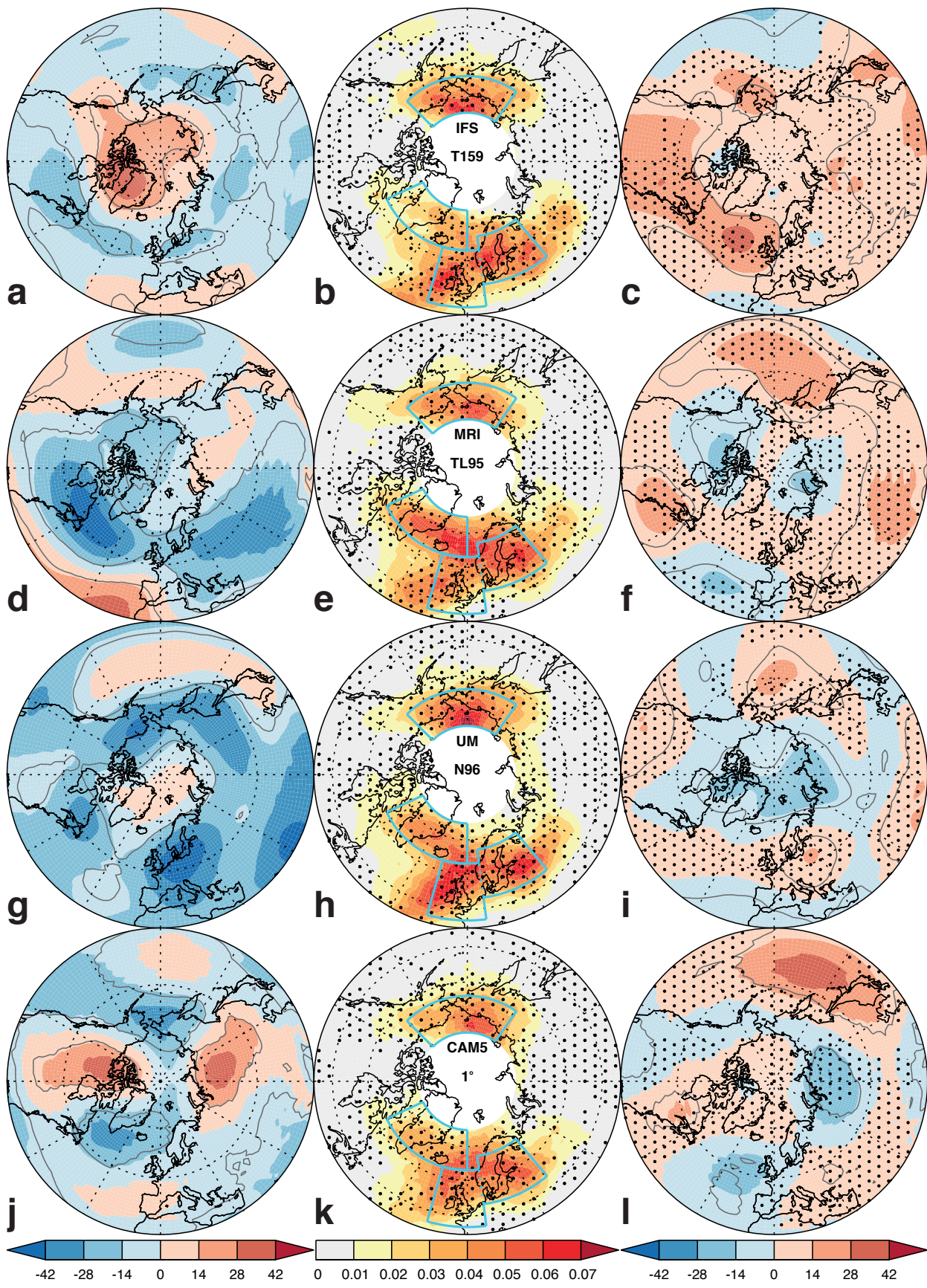


FIG. 14. As Fig. 13 but for spring (March–May).

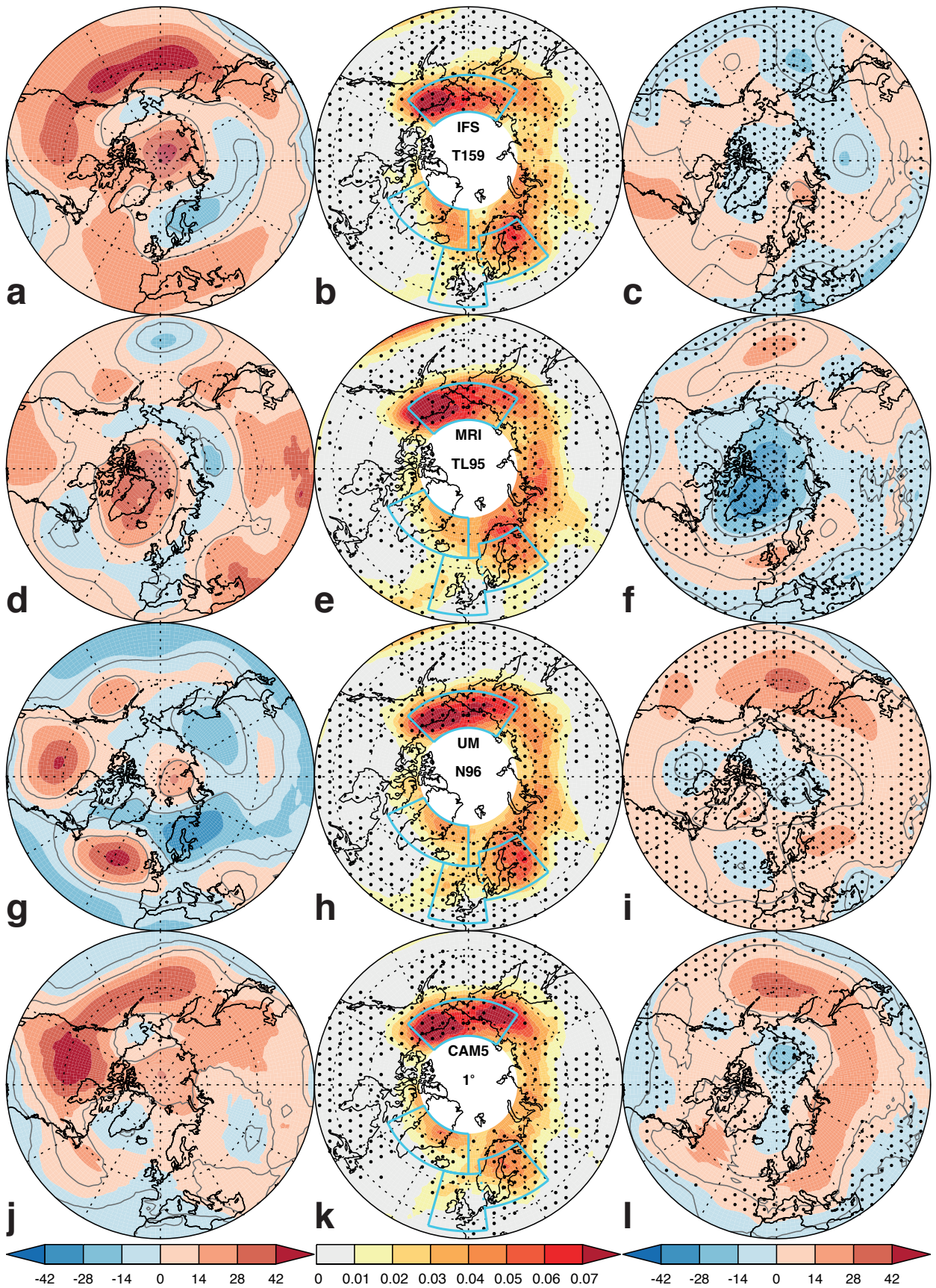


FIG. 15. As Fig. 13 but for summer (June–August).